

# Alleviating the Hubble Tension with a Local Void and Transitions of the Absolute Magnitude

Jing-Yi Jia <sup>a,\*</sup>, Jia-Lei Niu <sup>a</sup>, Da-Chun Qiang <sup>b</sup>, Hao Wei <sup>a,†</sup>

<sup>a)</sup> *School of Physics, Beijing Institute of Technology, Beijing 100081, China*

<sup>b)</sup> *Institute for Gravitational Wave Astronomy,  
Henan Academy of Sciences, Zhengzhou 450046, Henan, China*

## ABSTRACT

Nowadays, one of the well-known serious challenges in cosmology is the Hubble tension, namely the discrepancy between the Hubble constants from the local observation of Type Ia supernova (SNIa) and the high- $z$  observation of cosmic microwave background (CMB). Here, we are interested in alleviating the Hubble tension with a local void. The key idea is assuming that we live in a locally underdense void, where one will feel a faster expansion rate compared to the cosmic average. In the literature, it was found that a local void cannot satisfyingly alleviate the Hubble tension, since it is not preferred over the  $\Lambda$ CDM model by the observations such as the Pantheon SNIa sample, especially in terms of the information criteria AIC and BIC. In the present work, we try to alleviate the Hubble tension with a local void and transitions of the absolute magnitude  $M$ , by using the Pantheon+ SNIa sample alone or jointly with the CMB data of Planck 2018. We find that the Hubble tension can be satisfyingly alleviated, while the  $\Lambda$ LTB void models are strongly preferred by the observations.

PACS numbers: 98.80.Es, 98.65.Dx, 98.80.-k

---

\* email address: jjy@bit.edu.cn

† Corresponding author; email address: haowei@bit.edu.cn

## I. INTRODUCTION

Nowadays, one of the well-known serious challenges in cosmology is the Hubble tension [1–10]. That is, there is a significant tension between the Hubble constants  $H_0$  measured from various independent probes in the early and late/local universes. In particular, assuming the well-known  $\Lambda$ CDM model, the Hubble constant inferred from the final full-mission Planck measurements (Planck 2018) of the cosmic microwave background (CMB) is given by  $H_0 = 67.36 \pm 0.54$  km/s/Mpc [11]. Note that it cannot be substantially changed by assuming various trivial extensions to the base- $\Lambda$ CDM model. On the other hand, based on the Cepheid/Type Ia supernova (SNIa) distance ladder, the local determination of  $H_0$  from the Hubble Space Telescope (HST) and the SH0ES team (R22) is given by  $H_0 = 73.04 \pm 1.04$  km/s/Mpc [12]. Obviously, this Hubble constant directly from the local measurement of Cepheids/SNIa is in  $> 5\sigma$  tension with the one indirectly inferred from CMB in the early universe (at high redshift  $z_* \sim 1090$ ). Note that the recent SH0ES 2024 result (R24)  $H_0 = 73.17 \pm 0.86$  km/s/Mpc [13] is still in  $5 - 6\sigma$  tension with Planck 2018, while it has been cross-checked with the early James Webb Space Telescope (JWST) subsamples from SH0ES and CCHP.

In history, the Hubble tension has not emerged in the WMAP era of CMB before 2011, then manifested itself at  $2 - 3\sigma$  since the first Planck result in 2013, and finally reached  $> 5\sigma$  in December 2021 (R22). Various independent probes, e.g. the Tip of the Red Giant Branch (TRGB), Mira variables, J-region Asymptotic Giant Branch (JAGB) stars, baryon acoustic oscillations (BAO), strong gravitational lensing, gravitational waves, water masers, have been considered in the past decade to this end, but the Hubble tension has not been resolved to date. We refer to e.g. [1–10] for comprehensive reviews.

Many efforts have been made in the literature. Of course, it is fairly reasonable to carefully check the observational data, since there might be unresolved systematic errors in them. On the other hand, if all the observational data are right, the Hubble tension suggests the need for non-trivial extensions to the standard  $\Lambda$ CDM cosmology. There might be something new in the early, middle, late or local universes. Although numerous theoretical solutions have been proposed in the literature (e.g. [1–10, 113–118] and references therein), the Hubble tension is still a tough problem currently.

Here, we are interested in alleviating the Hubble tension with a local void. The key idea is to violate the cosmological principle by assuming that we live in a locally underdense void centered nearby our location. In this underdense region, one will feel a locally faster expansion rate compared to the cosmic average. Noting that  $H_0 \sim 73$  km/s/Mpc directly measured from the local Cepheids/SNIa is larger than  $H_0 \sim 67$  km/s/Mpc indirectly inferred from CMB assuming a background Friedmann-Robertson-Walker (FRW) universe, the Hubble tension might be alleviated with a local void [1, 2, 7, 8].

A local void can be approximately modeled by using the Lemaître-Tolman-Bondi (LTB) metric [14–16] firstly proposed in 1933, which is spherically symmetric and radially inhomogeneous. In 1998, the nearby sample has been examined for evidence of a local “Hubble Bubble” [17]. Later, various LTB void models were used to explain the cosmic acceleration without invoking dark energy or modified gravity [18–41]. Notice that cosmological constant is not allowed to this end, since it is the simplest candidate of dark energy as well known. Recently, the Hubble tension attracted a lot of attention. If the goal is no longer to explain the cosmic acceleration, we can allow a non-zero cosmological constant  $\Lambda$  in the LTB model and use the  $\Lambda$ LTB void model to alleviate the Hubble tension, while the cosmic acceleration is instead driven by  $\Lambda \neq 0$ . The role of LTB void has been changed in this case.

In 2013, the evidence for a  $\sim 300$  Mpc local void was claimed by Keenan, Barger and Cowie (KBC) [42]. In 2018, Hoscheit and Barger [43] claimed that the KBC void can significantly reduce the Hubble tension in the  $\Lambda$ LTB framework. Later in 2018, Shanks *et al.* [44] also claimed that a local void can satisfyingly relieve the Hubble tension. However, both results in [43, 44] were quickly criticized in 2019 by Kenworthy, Scolnic and Riess [45]. But the debate was not settled in fact. Luković *et al.* [46] continued the discussions in 2019, and Kazantzidis and Perivolaropoulos [47] claimed hints of a local void in 2020. At the end of 2020, Cai *et al.* [48] claimed again that the Hubble tension cannot be saved by a local void alone.

It is worth noting that the SNIa sample used in [43, 45–48] mentioned above is the Pantheon sample [49] released in 2017. But as is well known, the Hubble constant  $H_0$  is heavily degenerated with the absolute magnitude  $M$  of SNIa in the Pantheon sample (and other SNIa samples before Pantheon). Commonly, they can be marginalized as a combination  $\mathcal{M} = M + 5 \log(c/H_0/\text{Mpc}) + 25$  when we constrain other cosmological parameters, where  $c$  is the speed of light and “log” gives the logarithm to base 10. This is the reason to say “SNIa samples are Hubble-free” in the past. Thus, in order to infer the Hubble constant

$H_0$  from the Pantheon SNIa sample, the absolute magnitude  $M$  should be given *a priori* (usually the one from SH0ES is adopted). In the works of local (ALTB) void mentioned above, the absolute magnitude  $M$  of SNIa has also been given *a priori*, or  $M$  was fitted to data as a free parameter alternatively.

The situation has been changed since the Pantheon+ SNIa sample [50–52] released in 2022. In the Pantheon+ sample, the Cepheid calibrated host-galaxy distance moduli are also provided by SH0ES, which can be used to constrain the absolute magnitude  $M$ , and hence the degeneracy between  $H_0$  and  $M$  are broken. So,  $H_0$  and  $M$  can be separately constrained as free parameters. This makes the Pantheon+ sample much better than the Pantheon sample. On the other hand, the new Pantheon+ sample consists of more SNIa (especially more SNIa at low redshifts) than the old Pantheon sample. Thus, it is reasonable to study the Hubble tension with the Pantheon+ SNIa sample instead.

Interestingly, a bulk flow around  $z \sim 0.1$  and a local infall around  $z \sim 0.04$  were claimed by using the Pantheon+ SNIa sample in [53–55]. Similarly, the bulk flow in the local universe was also found with the Pantheon+ SNIa sample in [56] and with CosmicFlows4 in [57]. On the other hand, a local inhomogeneity was claimed in [58] with the Pantheon+ SNIa sample. In [59], a late-time inhomogeneous resolution for the Hubble tension with a chameleon dark energy was proposed. So, well motivated by these works, it is still interesting to consider a local inhomogeneity (especially a local void) for the Hubble tension in the new era of the Pantheon+ SNIa sample.

Usually, the absolute magnitude  $M$  of SNIa is assumed to be a universal constant, or two-value constants  $M = M_1$  for host stellar mass  $< 10^{10} M_\odot$  and  $M = M_2$  otherwise [49, 60, 61], where  $M_\odot$  is the solar mass. But this does not affect the cosmological constraints, since  $M$  will be marginalized with  $H_0$  as a combination  $\mathcal{M} = M + 5 \log(c/H_0/\text{Mpc}) + 25$  (see Appendix C of [62] for details). These are standard procedures for SNIa samples like Pantheon and before. However, the Pantheon+ sample is different, as mentioned above, in which  $H_0$  and  $M$  are separately constrained as free parameters. In [63], it is found that the absolute magnitude  $M$  in the Pantheon+ sample has a transition at the distance  $d_{\text{crit}} \sim 20$  Mpc, namely  $M = M_<$  for  $d < d_{\text{crit}}$  and  $M = M_>$  for  $d > d_{\text{crit}}$ , while the evidence is convincing in terms of  $\Delta\chi^2$  and the Akaike information criterion (AIC). Notice that this transition of  $M$  does not affect the constraints on other cosmological parameters e.g.  $\Omega_m$ , but slightly raises the best-fit  $H_0$ , and hence the Hubble tension cannot be addressed [63]. Recently, two transition models for the absolute magnitude  $M$  in the Pantheon+ sample were considered in [64], namely (a) sudden transition:  $M = M_0$  if  $z < z_t$  and  $M = M_0 + A$  if  $z \geq z_t$ , (b) linear transition:  $M(z) = M_0, M_0 + A(z - z_0)/(z_t - z_0), M_0 + A$  if  $z < z_0, z_0 \leq z < z_t, z \geq z_t$ , respectively. Notice that the transitions are given in terms of redshift  $z_t$ , rather than distance  $d_{\text{crit}}$  as in [63]. It was claimed in [64] that the Hubble tension could be alleviated by the sudden transition model with a mild evidence in terms of AIC (while the linear transition model failed in terms of AIC), but both the sudden and linear transition models failed in terms of the Bayesian information criterion (BIC).

Note that both [63, 64] are in the framework of  $\Lambda$ CDM cosmology, and they cannot alleviate the Hubble tension in terms of BIC (even in terms of AIC, the evidence for the sudden transition model in [64] is just “mild”, but not “strong”). Well motivated by the works mentioned above, we try to alleviate the Hubble tension with a local ALTb void and transitions of the absolute magnitude  $M$  in the present work. The evidence will be strong simultaneously in terms of  $\Delta\chi^2$ , AIC, BIC and Bayesian evidence.

The rest of this paper is organized as follows. In Sec. II, we briefly introduce the ALTb void model, which will be compared with the fiducial models in terms of the information criteria AIC and BIC. In Secs. III and IV, we test the models with the Pantheon+ SNIa sample, and SNIa plus CMB, respectively. We will see whether the Hubble tension can be alleviated by using the ALTb void models and transitions of the absolute magnitude  $M$ . Finally, a brief conclusion and some discussions are given in Sec. V.

## II. THE LOCAL ALTb VOID AND THE PRELIMINARY

### A. The local ALTb void

At first, we briefly introduce the ALTb void model, in which the universe is spherically symmetric and radially inhomogeneous, and we are living in a locally underdense void centered nearby our location. In comoving coordinates  $(r, \theta, \phi)$  and synchronous time  $t$ , the LTB metric is given by [14–16] (see also e.g. [24–32, 37, 43, 45, 48])

$$ds^2 = c^2 dt^2 - \frac{R'^2(r, t)}{1 - k(r)} dr^2 - R^2(r, t) d\Omega^2, \quad (1)$$

where  $c$  is the speed of light,  $d\Omega^2 = d\theta^2 + \sin^2 \theta d\phi^2$ , a prime denotes a derivative with respect to  $r$ , and  $k(r)$  is an arbitrary function of  $r$  playing the role of spatial curvature. Notice that it reduces to the well-known FRW metric if  $R(r, t) = a(t)r$  and  $k(r) = kr^2$ . Considering the universe filled by dust matter and a non-zero cosmological constant  $\Lambda$  (equivalently the vacuum energy), the Friedmann equation for the LTB model reads [26, 27, 30, 31, 43]

$$\frac{\dot{R}^2}{c^2} = -k(r) + \frac{2m(r)}{R} + \frac{\Lambda}{3} R^2, \quad (2)$$

where a dot denotes a derivative with respect to  $t$ . In fact, Eq. (2) is a first integral of the second Einstein field equation, and  $m(r)$  is arbitrary (non-negative) function of  $r$  from the integral, playing the role of gravitational mass within the comoving spherical shell. Introducing the Hubble parameter

$$H(r, t) \equiv \frac{\dot{R}(r, t)}{R(r, t)}, \quad (3)$$

and the fractional energy densities at the present time  $t_0$ ,

$$\Omega_m(r) \equiv \frac{2m(r)c^2}{H_0^2(r)R_0^3(r)}, \quad \Omega_k(r) \equiv \frac{-k(r)c^2}{H_0^2(r)R_0^2(r)}, \quad \Omega_\Lambda(r) \equiv \frac{\Lambda c^2}{3H_0^2(r)}, \quad (4)$$

where the subscript “0” indicates the value of corresponding quantity at the present time  $t_0$ , Eq. (2) evaluated at the present time  $t_0$  gives

$$1 = \Omega_m(r) + \Omega_k(r) + \Omega_\Lambda(r). \quad (5)$$

With Eq. (4), we can recast Eq. (2) as

$$H^2(r, t) = \left[ \frac{\dot{R}(r, t)}{R(r, t)} \right]^2 = H_0^2(r) \left[ \Omega_m(r) \frac{R_0^3(r)}{R^3(r, t)} + \Omega_k(r) \frac{R_0^2(r, t)}{R^2(r, t)} + \Omega_\Lambda(r) \right]. \quad (6)$$

Choosing the conventional gauge  $R(r, t_0) = R_0(r) = r$  (see e.g. [24–32, 37, 43, 45, 48]), it becomes

$$\dot{R}(r, t) = R(r, t) H_0(r) \left[ \Omega_m(r) \frac{r^3}{R^3(r, t)} + \Omega_k(r) \frac{r^2}{R^2(r, t)} + \Omega_\Lambda(r) \right]^{1/2}. \quad (7)$$

Note that Eq. (7) can be integrated and then inverted to solve for  $R(r, t)$  [45]. In order to compare the theoretical LTB model with observations, we need to associate the coordinates with redshift  $z$ . For an observer located at the center  $r = 0$ , by symmetry, incoming light travels along radial null geodesics,  $ds^2 = d\Omega^2 = 0$ , and hence we have [26–29, 37, 43, 45, 48]

$$\frac{dt}{dr} = -\frac{R'(r, t)}{c\sqrt{1 - k(r)}}. \quad (8)$$

On the other hand, the relation of the radial variable  $r$  to redshift  $z$  is given by [26–29, 37, 43, 45, 48]

$$\frac{1}{1+z} \frac{dz}{dr} = \frac{\dot{R}'(r, t)}{c\sqrt{1 - k(r)}}. \quad (9)$$

Eqs. (8) and (9) can be numerically integrated to find the cosmic time  $t$  and the radial coordinate  $r$  as functions of redshift  $z$  [45]. Finally, the luminosity distance is given by [26–29, 37, 43, 45, 48]

$$d_L(z) = (1+z)^2 R(r(z), t(z)). \quad (10)$$

To numerically solve the differential equations (7) – (9), the fractional densities  $\Omega_m(r)$ ,  $\Omega_k(r)$ ,  $\Omega_\Lambda(r)$  and their boundary conditions, as well as the boundary condition on  $H_0(r)$ , are needed [45].

Here, we consider a spherically symmetric local void surrounded by a flat  $\Lambda$ CDM background FRW universe. In this work, we use the (constrained) Garcia-Bellido-Haugboelle (GBH) profile function [28, 29] (see also e.g. [37, 43, 45, 48]) to model the mass distribution of the void, namely

$$\delta(r) = \delta_V \left[ \frac{1 - \tanh((r - r_V)/2\Delta_r)}{1 + \tanh(r_V/2\Delta_r)} \right], \quad (11)$$

with void depth  $\delta_V$ , void characteristic radius  $r_V$ , and transition width  $\Delta_r$  to uniformity. The fractional deficit  $\delta(r)$  is given by  $\delta(r) = (\Omega_m(r) - \Omega_{m,\text{out}})/\Omega_{m,\text{out}}$ , where the subscript “out” indicates the value (far) outside the void of corresponding quantity. Following e.g. [43, 48], we assume that  $\Omega_\Lambda(r)$  is constant. So, we have

$$\Omega_m(r) = \Omega_{m,\text{out}} (1 + \delta(r)), \quad \Omega_\Lambda(r) = 1 - \Omega_{m,\text{out}}, \quad \Omega_k(r) = 1 - \Omega_m(r) - \Omega_\Lambda(r). \quad (12)$$

Note that slightly different boundary conditions on  $\Omega_m(r)$  and  $\Omega_\Lambda(r)$  have been chosen in [45] (see its Appendix A for details). Nevertheless, in this work we use Eq. (12) following e.g. [43, 48], since they are extensively considered in the literature. On the other hand, the boundary condition on the time since the Big Bang  $t_B(r)$  is equivalent to the condition on  $H_0(r)$  [28, 29, 37, 43, 45, 48]. In the constrained GBH (CGBH) model [28, 29] (see also e.g. [37, 43, 45, 48]), it is assumed that the Big Bang is spatially homogeneous, namely  $t_B(r) = t_B = \text{const.}$ , which can be set to 0. Integrating Eq. (7), we find

$$t - t_B = t = \frac{1}{H_0(r)} \int_0^R \frac{dR}{R} \left[ \Omega_m(r) \frac{r^3}{R^3} + \Omega_k(r) \frac{r^2}{R^2} + \Omega_\Lambda(r) \right]^{-1/2}, \quad (13)$$

$$t_0 - t_B = t_0 = \frac{1}{H_0(r)} \int_0^r \frac{dR}{R} \left[ \Omega_m(r) \frac{r^3}{R^3} + \Omega_k(r) \frac{r^2}{R^2} + \Omega_\Lambda(r) \right]^{-1/2}, \quad (14)$$

in which we have used the gauge  $R_0 = r$  at  $t_0$ . On the other hand, outside the void, it is a flat  $\Lambda$ CDM background FRW universe, which easily leads to

$$t_0 - t_B = t_0 = \int_0^1 \frac{da}{H_{0,\text{out}} [\Omega_{m,\text{out}} a^{-1} + (1 - \Omega_{m,\text{out}}) a^2]^{1/2}}, \quad (15)$$

where  $a$  plays the role of scale factor outside the void. Following [48], we require that Eqs. (14) and (15) are equal, then obtain

$$H_0(r) = (t_0 - t_B)^{-1} \int_0^1 \frac{dx}{x} [\Omega_m(r) x^{-3} + \Omega_k(r) x^{-2} + \Omega_\Lambda(r)]^{-1/2}, \quad (16)$$

where  $x = R/r$  and  $t_0 - t_B$  is given by Eq. (15). Now we can numerically solve the differential equations (7) – (9) with  $H_0(r)$  given by Eq. (16) and  $k(r) = -r^2 H_0^2(r) \Omega_k(r)/c^2$  from Eq. (4). Then, using Eq. (10), the luminosity distance  $d_L(z)$  is ready to be confronted with the observational data.

## B. The fiducial models and the information criteria

The local ALTB void models should be compared with some fiducial models. In the present work, the first fiducial model is a flat  $\Lambda$ CDM model in the FRW universe, which is given by

$$E(z) \equiv H(z)/H_0 = \sqrt{\Omega_m (1+z)^3 + (1 - \Omega_m)}, \quad d_L(z) = (1+z) \frac{c}{H_0} \int_0^z \frac{d\tilde{z}}{E(\tilde{z})}, \quad (17)$$

and a constant absolute magnitude  $M$  is needed to fit the SNIa data. We label it as  $\Lambda\text{CDM}_F$  with three free model parameters  $\Omega_m$ ,  $H_0$  and  $M$ . The second fiducial model is also a flat  $\Lambda$ CDM model, but its

$\Delta\text{AIC}$			
Level of empirical support for the model with the smaller AIC			
0 – 2	4 – 7	> 10	
Weak	Mild	Strong	
$\Delta\text{BIC}$			
Evidence against the model with the larger BIC			
0 – 2	2 – 6	6 – 10	> 10
Weak	Positive	Strong	Very strong
$\ln \mathcal{B}$			
Evidence against the model with the smaller $\mathcal{Z}$			
0 – 1	1 – 2.5	2.5 – 5	> 5
Inconclusive	Weak	Moderate	Strong

TABLE I: The empirical strength of  $\Delta\text{AIC}$ ,  $\Delta\text{BIC}$  [69] (see also e.g. [63, 64]), and  $\ln \mathcal{B}$  [77] (see also e.g. [81]).

$\Omega_m = 0.3153$  and  $H_0 = 67.36$  km/s/Mpc are fixed by Planck 2018 result [11]. We label it as  $\Lambda\text{CDM}_{\text{P18}}$  with only one free model parameter  $M$ .

When we compare two models,  $\Delta\chi^2$  is not enough, since they might have different numbers of free model parameters. In the literature, a conventional criterion for model comparison is  $\chi^2/\text{dof}$ , where the degree of freedom  $\text{dof} = N - \kappa$ , while  $N$  and  $\kappa$  are the number of data points and the number of free model parameters, respectively. The most sophisticated criterion is the Bayesian evidence (see e.g. [65, 66] and references therein). But the computation of Bayesian evidence usually consumes a large amount of time and power. As an alternative, some approximations of Bayesian evidence such as the information criteria AIC and BIC have been extensively used in the literature. The AIC is defined by [67]

$$\text{AIC} = -2 \ln \mathcal{L}_{\max} + 2\kappa, \quad (18)$$

where  $\mathcal{L}_{\max}$  is the maximum likelihood. In the Gaussian cases,  $\chi_{\min}^2 = -2 \ln \mathcal{L}_{\max}$ . The BIC is defined by [68]

$$\text{BIC} = -2 \ln \mathcal{L}_{\max} + \kappa \ln N. \quad (19)$$

Comparing Eqs. (18) and (19), it is easy to see that BIC is tougher than AIC for  $\ln N > 2$ . Notice that the Pantheon+ SNIa sample consists of 1701 data points and  $\ln N \sim 7.44 \gg 2$ . Actually, this is the deep reason for the failures of [63, 64] in terms of BIC, as mentioned above. Usually, a smaller AIC or BIC means a better fitting for the given model, and we compare two models by calculating the differences in AIC and BIC. In this work, we will calculate  $\Delta\text{AIC}$  and  $\Delta\text{BIC}$  for the  $\Lambda\text{LTB}$  models relative to two fiducial  $\Lambda\text{CDM}$  models. A negative (positive) value of  $\Delta\text{AIC}$  or  $\Delta\text{BIC}$  means a preference for the  $\Lambda\text{LTB}$  ( $\Lambda\text{CDM}$ ) model. Notice that the strength of evidence is indicated by the empirical ranges of  $|\Delta\text{AIC}|$  or  $|\Delta\text{BIC}|$  summarized in Table I [69] (see also e.g. [63, 64]). Finally, we also consider the Bayesian evidence and the Bayes factor (see e.g. [76–80]) for model comparison. The Bayesian evidence is defined by

$$\mathcal{Z} = \int \mathcal{L}(\psi) P(\psi) d\psi, \quad (20)$$

where  $\mathcal{L}$  is the likelihood function,  $P$  is the prior distribution, and  $\psi$  denotes the model parameters. For model comparison, it is convenient to use the Bayes factor

$$\mathcal{B}_{12} = \mathcal{Z}_1 / \mathcal{Z}_2, \quad \text{or equivalently,} \quad \ln \mathcal{B}_{12} = \ln \mathcal{Z}_1 - \ln \mathcal{Z}_2, \quad (21)$$

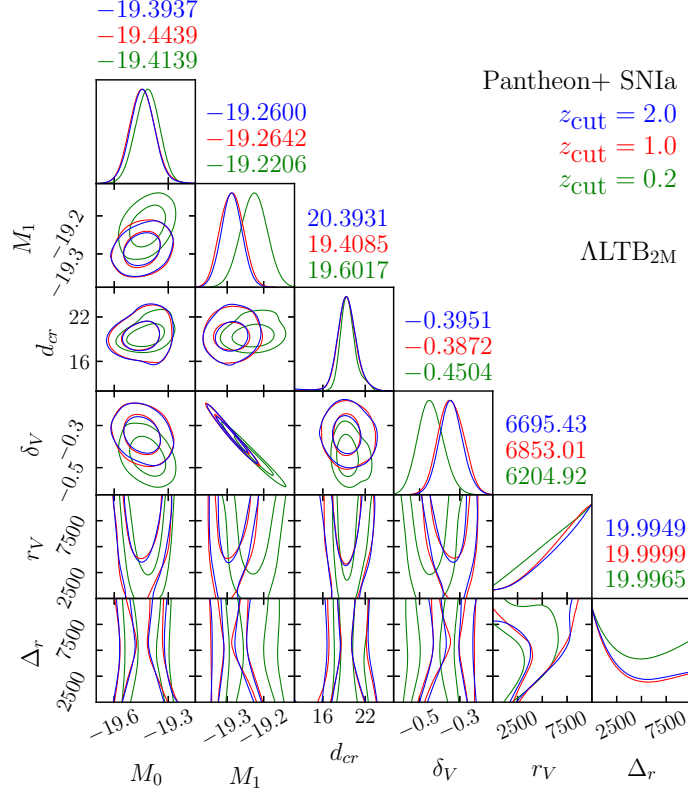


FIG. 1: The  $1\sigma$  and  $2\sigma$  contours for all the free parameters of the ALTB model with a transition of the absolute magnitude  $M$ , i.e. the ALTB<sub>2M</sub> model, from three  $z < z_{\text{cut}}$  subsets with  $z_{\text{cut}} = 0.2$  (green),  $1.0$  (red),  $2.0$  (blue) of the Pantheon+ SNIa sample. The marginalized probability distributions and the best-fit values are also given at the tops of all columns for the corresponding parameters. The quantities of length e.g.  $d_{cr}$ ,  $r_V$  and  $\Delta_r$  are in units of Mpc. See Sec. III for details.

where  $\mathcal{Z}_1$  and  $\mathcal{Z}_2$  are the Bayesian evidences for models  $Q_1$  and  $Q_2$ , respectively. If  $\mathcal{B}_{12}$  is larger (smaller) than 1, model  $Q_1$  ( $Q_2$ ) is preferred over the other model. Here, we will also compute  $\ln \mathcal{B}$  for the ALTB models relative to two fiducial  $\Lambda$ CDM models. A positive (negative) value of  $\ln \mathcal{B}$  means a preference for the ALTB ( $\Lambda$ CDM) model. The strength of evidence is also indicated by the empirical ranges of  $|\ln \mathcal{B}|$  summarized in Table I [77] (see also e.g. [81]). Note that one can compute the Bayesian evidence by using the nested sampling (such as PolyChord, dynesty, MultiNest, nessai), or alternatively MCEvidence with the MCMC chains [82–84].

### III. TESTING THE MODELS WITH THE PANTHEON+ SNIA SAMPLE

In this work, we are interested in alleviating the Hubble tension with a local ALTB void. To this end, the conditions  $\Omega_{m,\text{out}} = 0.3153$  and  $H_{0,\text{out}} = 67.36$  km/s/Mpc for the ALTB models should be adopted to match the CMB observations of Planck 2018 [11], as in e.g. [48]. So, the local universe can be described by a ALTB model inside the void (and outside the void nearby), while the background universe can be described by a flat  $\Lambda$ CDM<sub>P18</sub> model far outside the void. The cosmology smoothly transits between them through the tanh function in GBH profile given by Eq. (11).

The Pantheon+ SNIa sample [50–52] consists of 1701 light curves of 1550 SNIa at redshifts  $0.00122 \leq z \leq 2.26137$  (in this work we use the Hubble diagram redshifts  $z_{\text{HD}}$  given by column 3 of the Pantheon+ data table with CMB and peculiar velocity corrections). Only one of them is at redshift  $z > 2$ . Notice that 77 Cepheid calibrated host-galaxy distance moduli are also provided by SH0ES (many of them are duplicate) at redshifts  $0.00122 \leq z \leq 0.01682$  (only 10 of them are at  $z > 0.01$ ).

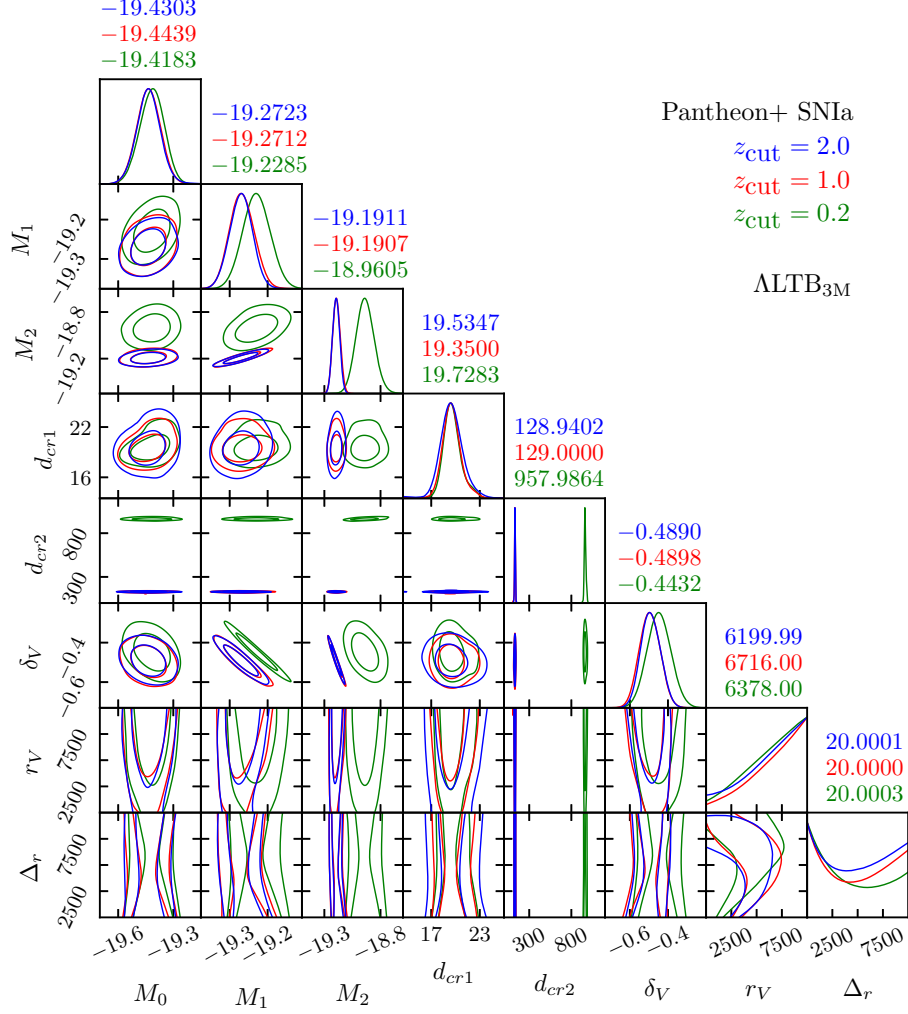


FIG. 2: The same as in Fig. 1, but for the ALTB<sub>3M</sub> model. See Sec. III for details.

Following [50], the cosmological parameters are constrained with Pantheon+ SNIa by minimizing

$$\chi_{\text{SN}}^2 = \Delta\boldsymbol{\mu}^T \cdot \mathbf{C}_{\text{stat+sys}}^{-1} \cdot \Delta\boldsymbol{\mu}, \quad (22)$$

where  $\mathbf{C}_{\text{stat+sys}}$  is the covariance matrix including statistical and systematic uncertainties,  $\Delta\boldsymbol{\mu}$  is the vector of 1701 SNIa distance modulus residuals computed as

$$\Delta\mu_i = \begin{cases} \mu_i - \mu_i^{\text{Ceph}} & i \in \text{Cepheid hosts}, \\ \mu_i - \mu_{\text{model}}(z_i) & \text{otherwise}, \end{cases} \quad (23)$$

in which  $\mu_i = m_{B,i} - M$  is the distance modulus of the  $i$ -th SNIa,  $M$  is the absolute magnitude,  $\mu_i^{\text{Ceph}}$  is the Cepheid calibrated host-galaxy distance modulus provided by SH0ES,  $m_{B,i}$  is the corrected/standardized apparent magnitude, and the model distance modulus  $\mu_{\text{model}}(z_i)$  is given by

$$\mu_{\text{model}}(z_i) = 5 \log(d_L(z_i)/\text{Mpc}) + 25, \quad (24)$$

while  $d_L(z)$  is the luminosity distance predicted by the model, and “log” gives the logarithm to base 10. We minimize  $\chi_{\text{SN}}^2$  by using the Markov Chain Monte Carlo (MCMC) Python package Cobaya [70, 71] with GetDist [72, 73], and then obtain the constraints on the model parameters.



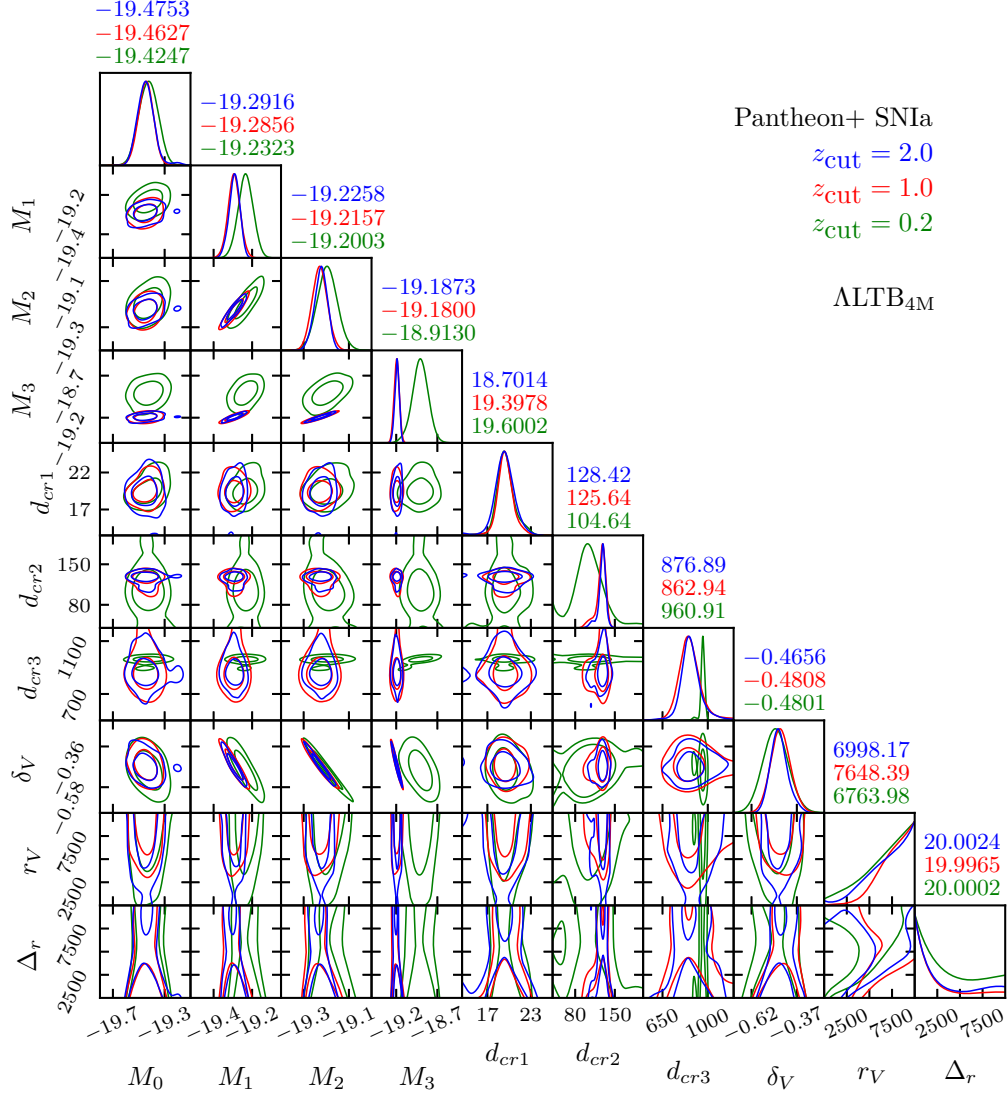


FIG. 3: The same as in Fig. 1, but for the  $\text{ALTB}_{4M}$  model. See Sec. III for details.

Following [48], we consider three subsets of the Pantheon+ SNIa sample, namely three  $z < z_{\text{cut}}$  subsets with  $z_{\text{cut}} = 0.2, 1.0, 2.0$ , respectively. Note that the case of  $z < 2.0$  is almost the full Pantheon+ sample, since there is only one SNIa at redshift  $z > 2$ . In the following, we test the models with these three SNIa subsets consisting of 948, 1676, 1700 data points, respectively.

For the following model comparison, we fit the fiducial  $\Lambda\text{CDM}_{\text{F}}$  model to three  $z < z_{\text{cut}}$  SNIa subsets with  $z_{\text{cut}} = 0.2, 1.0, 2.0$ , and find  $\chi^2_{\text{SN}, \text{min}, \text{F}} = 901.516, 1500.854, 1522.907$ , respectively. For the fiducial  $\Lambda\text{CDM}_{\text{P18}}$  model,  $\chi^2_{\text{SN}, \text{min}, \text{P18}} = 943.442, 1546.216, 1565.501$ , respectively.

Actually, we have tried the ALTB model with a universal absolute magnitude  $M$ , and found that the Pantheon+ SNIa sample does not prefer it over the fiducial  $\Lambda\text{CDM}$  models in terms of AIC and BIC. On the other hand, hints for a transition of the absolute magnitude  $M$  of SNIa have been found in [63, 64], as mentioned above. Motivated by this, here we consider the ALTB model with a transition of the absolute magnitude  $M$ . Following [63], we assume a transition of  $M$  at a critical distance  $d_{\text{cr}}$  (associated with a critical distance modulus  $\mu_{\text{cr}} = 5 \log(d_{\text{cr}}/\text{Mpc}) + 25$ ), namely

$$M = \begin{cases} M_0 & \text{if } \mu_{i, \text{S}} < \mu_{\text{cr}}, \\ M_1 & \text{if } \mu_{i, \text{S}} \geq \mu_{\text{cr}}, \end{cases} \quad (25)$$

Model	$M_0$	$M_1$	$M_2$	$M_3$	$d_{cr1}$	$d_{cr2}$	$d_{cr3}$	$\delta_V$	$r_V$	$\Delta_r$
$z < 0.2$										
ALTB <sub>2M</sub>	$-19.42^{+0.06}_{-0.06}$	$-19.23^{+0.03}_{-0.03}$			$19.57^{+0.59}_{-0.99}$			$-0.44^{+0.05}_{-0.06}$	$> 5403.66$	none
ALTB <sub>3M</sub>	$-19.42^{+0.06}_{-0.05}$	$-19.23^{+0.03}_{-0.03}$	$-18.94^{+0.06}_{-0.07}$		$19.64^{+0.57}_{-1.04}$	$962.92^{+7.69}_{-9.40}$		$-0.45^{+0.05}_{-0.05}$	$> 5431.18$	none
ALTB <sub>4M</sub>	$-19.42^{+0.06}_{-0.06}$	$-19.23^{+0.03}_{-0.03}$	$-19.20^{+0.04}_{-0.04}$	$-18.91^{+0.09}_{-0.07}$	$19.60^{+0.56}_{-1.05}$	$103.63^{+21.91}_{-10.53}$	$959.23^{+11.18}_{-5.55}$	$-0.49^{+0.06}_{-0.06}$	$> 5763.84$	none
$z < 1.0$										
ALTB <sub>2M</sub>	$-19.44^{+0.05}_{-0.06}$	$-19.29^{+0.03}_{-0.03}$			$19.34^{+0.84}_{-0.89}$			$-0.36^{+0.05}_{-0.06}$	$> 6573.41$	none
ALTB <sub>3M</sub>	$-19.43^{+0.06}_{-0.06}$	$-19.27^{+0.03}_{-0.03}$	$-19.19^{+0.03}_{-0.03}$		$19.61^{+0.58}_{-1.00}$	$129.02^{+3.43}_{-3.58}$		$-0.49^{+0.05}_{-0.05}$	$> 5838.62$	none
ALTB <sub>4M</sub>	$-19.45^{+0.06}_{-0.06}$	$-19.29^{+0.03}_{-0.03}$	$-19.23^{+0.03}_{-0.03}$	$-19.19^{+0.03}_{-0.03}$	$19.43^{+0.69}_{-0.91}$	$126.90^{+6.21}_{-2.26}$	$865.56^{+22.58}_{-70.62}$	$-0.46^{+0.05}_{-0.05}$	$> 7091.30$	$< 1699.04$
$z < 2.0$										
ALTB <sub>2M</sub>	$-19.44^{+0.06}_{-0.06}$	$-19.29^{+0.02}_{-0.02}$			$19.73^{+0.82}_{-0.81}$			$-0.37^{+0.05}_{-0.05}$	$> 6401.97$	none
ALTB <sub>3M</sub>	$-19.44^{+0.05}_{-0.05}$	$-19.27^{+0.03}_{-0.03}$	$-19.19^{+0.03}_{-0.03}$		$19.45^{+0.71}_{-0.87}$	$129.40^{+3.06}_{-3.84}$		$-0.49^{+0.04}_{-0.05}$	$> 5535.31$	none
ALTB <sub>4M</sub>	$-19.45^{+0.06}_{-0.06}$	$-19.29^{+0.03}_{-0.03}$	$-19.23^{+0.03}_{-0.03}$	$-19.19^{+0.03}_{-0.03}$	$19.13^{+1.01}_{-0.65}$	$127.20^{+7.30}_{-2.06}$	$879.04^{+16.57}_{-88.82}$	$-0.46^{+0.05}_{-0.05}$	$> 6354.77$	none

TABLE II: The means and  $1\sigma$  uncertainties for all the free parameters of the ALTB models from the subsets  $z < z_{\text{cut}}$  with  $z_{\text{cut}} = 0.2, 1.0, 2.0$  of the Pantheon+ SNIa sample. Note that  $d_{cr1}$  should be regarded as  $d_{cr}$  in the ALTB<sub>2M</sub> model. The quantities of length e.g.  $d_{cr, i}$ ,  $r_V$  and  $\Delta_r$  are in units of Mpc. In the last column, “none” indicates that the corresponding model parameter cannot be well constrained by the data. See Sec. III for details.

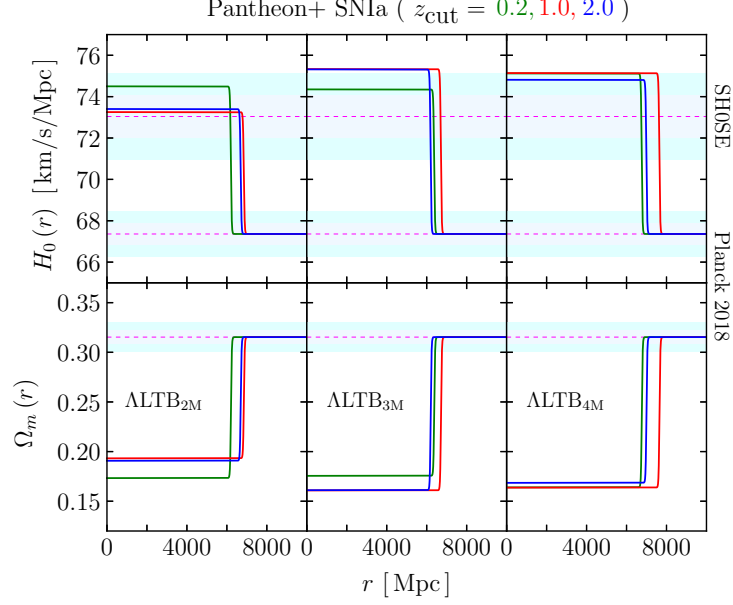


FIG. 4:  $H_0(r)$  and  $\Omega_m(r)$  of the  $\text{ALT}_{\text{B}2\text{M}}$  (left),  $\text{ALT}_{\text{B}3\text{M}}$  (middle),  $\text{ALT}_{\text{B}4\text{M}}$  (right) void models as functions of the radial variable  $r$  plotted with the best-fit parameters from three  $z < z_{\text{cut}}$  subsets with  $z_{\text{cut}} = 0.2$  (green), 1.0 (red), 2.0 (blue) of the Pantheon+ SNIa sample. The  $1\sigma$ ,  $2\sigma$  uncertainties and median values of  $H_0$  from SH0ES,  $H_0$  and  $\Omega_m$  from Planck 2018, are also shown by the shaded regions with dashed lines. See Sec. III for details.

Model	$\chi^2_{\text{SN}, \text{min}}$	$\chi^2_{\text{SN}, \text{min}}/\text{dof}$	$\Delta\text{BIC}_{\text{F}}$	$\Delta\text{AIC}_{\text{F}}$	$\Delta\chi^2_{\text{F}}$	$\ln \mathcal{B}_{\text{F}}$	$\Delta\text{BIC}_{\text{P18}}$	$\Delta\text{AIC}_{\text{P18}}$	$\Delta\chi^2_{\text{P18}}$	$\ln \mathcal{B}_{\text{P18}}$
$z < 0.2$										
$\text{ALT}_{\text{B}2\text{M}}$	887.96	0.9426	7.01	-7.55	-13.55	2.06	-21.21	-45.48	-55.48	17.42
$\text{ALT}_{\text{B}3\text{M}}$	854.01	0.9085	-13.23	-37.50	-47.50	11.89	-41.45	-75.43	-89.43	27.25
$\text{ALT}_{\text{B}4\text{M}}$	847.55	0.9036	-5.99	-39.97	-53.97	12.03	-34.20	-77.89	-95.89	27.39
$z < 1.0$										
$\text{ALT}_{\text{B}2\text{M}}$	1497.16	0.8965	18.58	2.31	-3.69	-2.38	-11.93	-39.05	-49.05	14.10
$\text{ALT}_{\text{B}3\text{M}}$	1468.56	0.8804	4.83	-22.29	-32.29	1.37	-25.68	-63.65	-77.65	17.86
$\text{ALT}_{\text{B}4\text{M}}$	1456.58	0.8743	7.70	-30.27	-44.27	3.44	-22.82	-71.63	-89.63	19.93
$z < 2.0$										
$\text{ALT}_{\text{B}2\text{M}}$	1515.38	0.8946	14.78	-1.53	-7.53	-0.16	-12.93	-40.12	-50.12	14.63
$\text{ALT}_{\text{B}3\text{M}}$	1486.69	0.8787	0.98	-26.22	-36.22	3.58	-26.74	-64.81	-78.81	18.37
$\text{ALT}_{\text{B}4\text{M}}$	1474.91	0.8727	4.07	-34.00	-48.00	3.54	-23.65	-72.60	-90.60	18.33

TABLE III: The model comparison of various ALTB void models relative to the fiducial  $\Lambda\text{CDM}_{\text{F}}$  and  $\Lambda\text{CDM}_{\text{P18}}$  models (labeled by the subscripts “F” and “P18” respectively), by using the subsets  $z < z_{\text{cut}}$  with  $z_{\text{cut}} = 0.2, 1.0, 2.0$  of the Pantheon+ SNIa sample. See Sec. III for details.

where  $\mu_{i, \text{S}}$  is given by column 11 of the Pantheon+ data table (note that it is roughly inferred by using the SH0ES absolute magnitude, and hence  $\mu_{i, \text{S}}$  cannot be used for cosmological constraints [50–52]). We label this model as  $\text{ALT}_{\text{B}2\text{M}}$ .

It is natural to imagine that the absolute magnitude  $M$  has many transitions, which are very reasonable generalizations. In the ALTB void model, if  $M$  have two transitions at the critical distances  $d_{\text{cr}1}$  and  $d_{\text{cr}2}$  (associated with the critical distance moduli  $\mu_{\text{cr}1, 2} = 5 \log(d_{\text{cr}1, 2}/\text{Mpc}) + 25$ ), namely

$$M = \begin{cases} M_0 & \text{if } \mu_{i,S} < \mu_{cr1}, \\ M_1 & \text{if } \mu_{cr1} \leq \mu_{i,S} < \mu_{cr2}, \\ M_2 & \text{if } \mu_{i,S} \geq \mu_{cr2}, \end{cases} \quad (26)$$

we label this model as  $\text{ALTB}_{3M}$ . Similarly, if  $M$  have three transitions at the critical distances  $d_{cr1}$ ,  $d_{cr2}$  and  $d_{cr3}$  (associated with the critical distance moduli  $\mu_{cr1,2,3} = 5 \log(d_{cr1,2,3}/\text{Mpc}) + 25$ ) in the  $\text{ALTB}$  void model, namely

$$M = \begin{cases} M_0 & \text{if } \mu_{i,S} < \mu_{cr1}, \\ M_1 & \text{if } \mu_{cr1} \leq \mu_{i,S} < \mu_{cr2}, \\ M_2 & \text{if } \mu_{cr2} \leq \mu_{i,S} < \mu_{cr3}, \\ M_3 & \text{if } \mu_{i,S} \geq \mu_{cr3}, \end{cases} \quad (27)$$

we label it as  $\text{ALTB}_{4M}$ . More transitions of  $M$  are not worthy, and hence we stop here.

We fit the  $\text{ALTB}_{2M}$ ,  $\text{ALTB}_{3M}$ ,  $\text{ALTB}_{4M}$  void models to three  $z < z_{\text{cut}}$  subsets with  $z_{\text{cut}} = 0.2, 1.0, 2.0$  of the Pantheon+ SNIa sample, and present the  $1\sigma$  and  $2\sigma$  constraints on their free model parameters in Figs. 1 – 3, respectively. Notice that the best-fit values of their model parameters are also given in these figures. Although the marginalized probability distributions and the  $1\sigma$ ,  $2\sigma$  contours of all the free model parameters have been plotted in Figs. 1 – 3, we also explicitly give their numerical means and  $1\sigma$  intervals in Table II. On the other hand, we present their best-fit  $\chi^2_{\text{SN},\text{min}}$  and  $\chi^2_{\text{SN},\text{min}}/\text{dof}$  in Table III. Then, we calculate their  $\Delta\chi^2$ ,  $\Delta\text{AIC}$ ,  $\Delta\text{BIC}$ ,  $\ln\mathcal{B}$  relative to the fiducial  $\Lambda\text{CDM}_{\text{F}}$  and  $\Lambda\text{CDM}_{\text{P18}}$  models (labeled by the subscripts “F” and “P18” respectively), and also present them in Table III. In Fig. 4, we plot  $H_0(r)$  and  $\Omega_m(r)$  as functions of the comoving distance  $r$  by using the best-fit model parameters given in Figs. 1 – 3.

From Fig. 4, one can easily find the local Hubble constant  $H_{0,\text{in}} = H_0(r=0)$  at the center  $r=0$  (where we live) for the  $\text{ALTB}$  void models, which will be compared with the one measured by SH0ES (as shown by the upper shaded regions with a dashed line in Fig. 4). Far outside the void, it is clear to see that all the  $H_0(r)$  at large  $r$  of three  $\text{ALTB}$  models match  $H_{0,\text{out}} = 67.36 \text{ km/s/Mpc}$  from the CMB observation of Planck 2018 (as shown by the lower shaded regions with a dashed line in Fig. 4). Actually, this is the very condition imposed at the beginning of Sec. III. Obviously, in the  $\text{ALTB}_{2M}$  model, its local  $H_{0,\text{in}} = H_0(r=0)$  perfectly closes to the median value  $H_0 = 73.04 \text{ km/s/Mpc}$  of SH0ES for the cases of  $z_{\text{cut}} = 1.0, 2.0$ , and falls into  $2\sigma$  region of SH0ES in the case of  $z_{\text{cut}} = 0.2$ . On the other hand, in the  $\text{ALTB}_{3M}$  and  $\text{ALTB}_{4M}$  models, their  $H_{0,\text{in}} = H_0(r=0)$  fall into  $2\sigma$  region of SH0ES in all cases. So, all the three  $\text{ALTB}$  void models can significantly alleviate the Hubble tension, as expected.

From Figs. 1 – 3 and Table II, we can see that the characteristic radius  $r_V$  and transition width  $\Delta_r$  of the voids cannot be well constrained by the Pantheon+ SNIa sample. Note that in all the three  $\text{ALTB}$  void models the best-fit  $\Delta_r \sim 20 \text{ Mpc} \ll r_V$  is fairly short, and hence  $\Omega_m(r)$  and  $H_0(r)$  transit the edge of the local void around  $r_V$  steeply, as shown in Fig. 4. On the other hand, the void depth (fractional deficit)  $\delta_V$  can be well constrained in all the three  $\text{ALTB}$  void models, and they can be  $\delta_V \lesssim -38\%$ , even  $\lesssim -48\%$ , as shown in Figs. 1 – 3 and Table II. This also can be seen from Fig. 4 that the local  $\Omega_{m,\text{in}} = \Omega_m(r=0) < 0.2$  is about  $(1 + \delta_V) \Omega_{m,\text{out}} = (1 - 38\%) \times 0.3153 \sim 0.2$  or even smaller. As noted in [48],  $\delta_V \lesssim -30\%$  is required to alleviate the Hubble tension, but they failed by using the Pantheon SNIa sample. With the help of transitions of the absolute magnitude  $M$ , we can satisfyingly make  $\delta_V \lesssim -38\%$  or even smaller in the present work by using the Pantheon+ SNIa sample. This is the key to alleviate the Hubble tension with a local void.

On the other hand, from Figs. 1 – 3 we find a transition of the absolute magnitude  $M$  at  $\sim 20 \text{ Mpc}$  in all models. Thus, we independently confirm this point found in [63] previously. In the present work, we further find two transitions of the absolute magnitude  $M$  at  $\sim 129 \text{ Mpc}$  and  $\sim 860 - 960 \text{ Mpc}$ . Meanwhile, we find in all the three  $\text{ALTB}$  void models that the segmented  $M_i$  becomes higher as the distance increases (namely  $M_3 > M_2 > M_1 > M_0$  at the critical distances  $d_{cr3} > d_{cr2} > d_{cr1}$ ), as shown in Figs. 1 – 3. So, if the absolute magnitude  $M = M(d)$  or  $M(z)$ , it might be a (monotone) increasing function.

From Table II, we can see that the constraints on the free model parameters are fairly tight (except  $r_V$  and  $\Delta_r$ ). We stress that the transitions of the absolute magnitude  $M$  are statistically significant (far

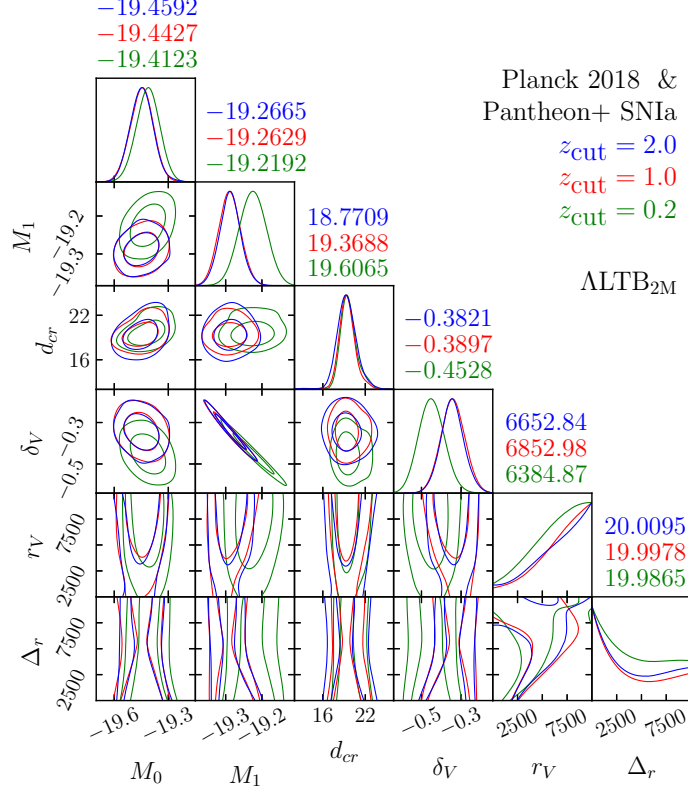


FIG. 5: The same as in Fig. 1, but for the ALTB<sub>2M</sub> model and the data of SNIa+CMB. See Sec. IV for details.

beyond  $1\sigma$  uncertainties). They are not apparent changes due to large errors. On the other hand, despite the void parameters  $r_V$  and  $\Delta_r$  cannot be well constrained, they do not affect the main results since the key void parameter  $\delta_V$  can be tightly constrained in fact.

From Table III, it is easy to see that all the three ALTB models are strongly preferred over the fiducial  $\Lambda\text{CDM}_{\text{P18}}$  model with “very strong”  $\Delta\chi^2_{\text{P18}}$ ,  $\Delta\text{AIC}_{\text{P18}}$ ,  $\Delta\text{BIC}_{\text{P18}}$  and  $\ln\mathcal{B}_{\text{P18}}$  evidences. On the other hand, the ALTB<sub>3M</sub> and ALTB<sub>4M</sub> models are preferred over the fiducial  $\Lambda\text{CDM}_{\text{F}}$  model with “very strong”  $\Delta\text{AIC}_{\text{F}}$  and  $\Delta\chi^2_{\text{F}}$  evidences in all cases, while the ALTB<sub>2M</sub> model is mildly preferred over the fiducial  $\Lambda\text{CDM}_{\text{F}}$  model. However, they fail in many cases with positive  $\Delta\text{BIC}_{\text{F}}$  relative to the fiducial  $\Lambda\text{CDM}_{\text{F}}$  model, as shown by the 4th column of Table III. So, in terms of BIC, the ALTB void models are still not preferred over the fiducial  $\Lambda\text{CDM}_{\text{F}}$  model, by using the Pantheon+ SNIa sample alone. Even in terms of  $\ln\mathcal{B}_{\text{F}}$ , the ALTB void models are only preferred over the fiducial  $\Lambda\text{CDM}_{\text{F}}$  model with “moderate” evidences in many cases, and fail with weakly negative  $\ln\mathcal{B}_{\text{F}}$  in two cases. Thus, we still cannot claim a full triumph so far.

#### IV. TESTING THE MODELS WITH SNIa AND CMB

It is worth noting that the conditions  $\Omega_{m,\text{out}} = 0.3153$  and  $H_{0,\text{out}} = 67.36$  km/s/Mpc for the ALTB models have been imposed with the strong intention of reconciling the discrepancy between the local observation of SNIa and the high- $z$  observation of CMB, as mentioned at the beginning of Sec. III. If one only uses the SNIa data, it is not necessary to impose these conditions on  $\Omega_{m,\text{out}}$  and  $H_{0,\text{out}}$ , and they should be regarded as free model parameters. It is unfair to impose these conditions without using the CMB data. In other words, when we impose these conditions on  $\Omega_{m,\text{out}}$  and  $H_{0,\text{out}}$ , the CMB data must be also taken into account, jointly with the SNIa data.

It consumes a large amount of time and power to use the full CMB data. As an alternative, the distance priors derived from the full CMB data have been extensively used the literature, which contain the main

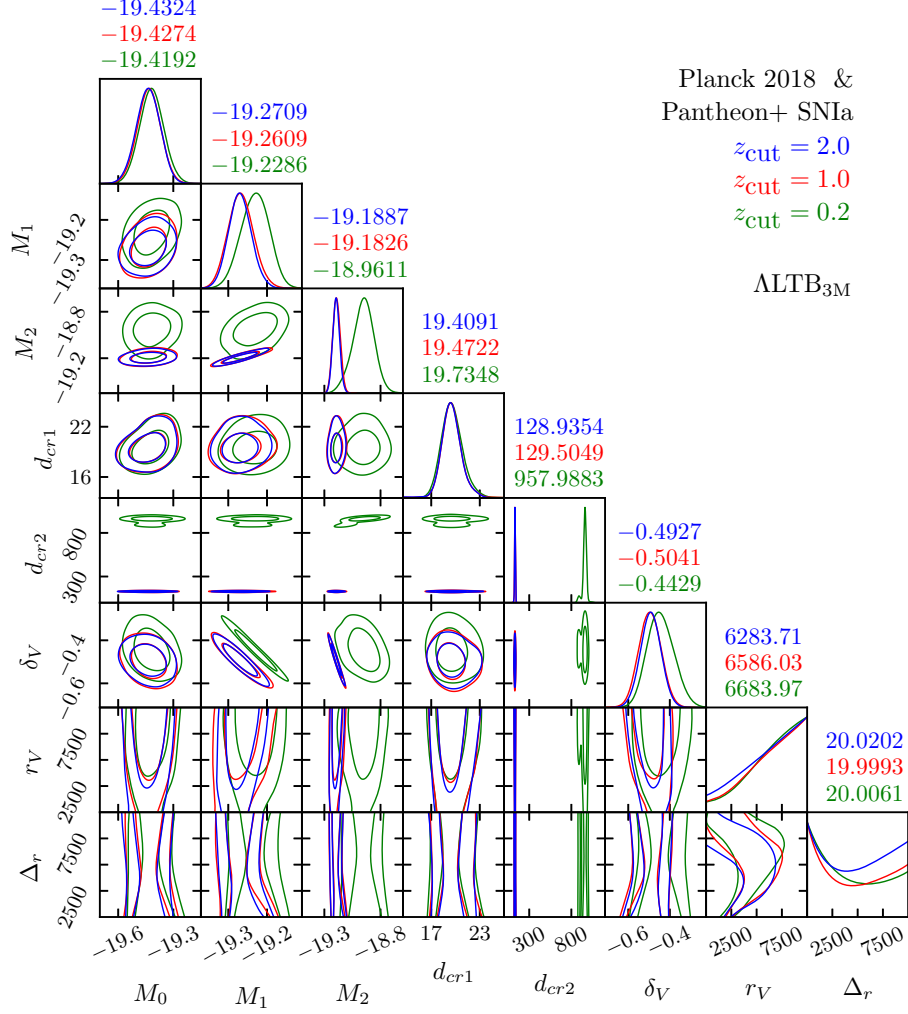


FIG. 6: The same as in Fig. 1, but for the ALTB<sub>3M</sub> model and the data of SNIa+CMB. See Sec. IV for details.

information of CMB. Here, we consider the distance priors in [74] derived from the CMB observation of Planck 2018. In this case, the  $\chi^2$  for CMB is given by [74]

$$\chi_{\text{CMB}}^2 = \Delta \mathbf{d}^T \cdot \mathbf{C}_d^{-1} \cdot \Delta \mathbf{d}, \quad (28)$$

where  $\Delta \mathbf{d}$  is the vector of distance prior residuals, and  $\mathbf{C}_d^{-1}$  is the inverse covariance matrix, namely

$$\Delta \mathbf{d} = \begin{pmatrix} \mathcal{R}_{\text{model}}(z_*) - 1.750235 \\ \ell_{A, \text{model}}(z_*) - 301.4707 \end{pmatrix}, \quad \mathbf{C}_d^{-1} = \begin{pmatrix} 94392.3971 & -1360.4913 \\ -1360.4913 & 161.4349 \end{pmatrix}, \quad (29)$$

in which  $z_* = 1089.92$  from the Planck 2018 result [11]. The shift parameter  $\mathcal{R}$  is given by

$$\mathcal{R}_{\text{model}}(z_*) = (H_0/c) \sqrt{\Omega_m} (1 + z_*) d_A(z_*), \quad (30)$$

and the acoustic scale  $\ell_A$  is given by

$$\ell_{A, \text{model}}(z_*) = (1 + z_*) \pi d_A(z_*) / r_s(z_*), \quad (31)$$

where  $d_A(z) = (1+z)^{-2} d_L(z)$  is the angular diameter distance, which can be obtained from the luminosity

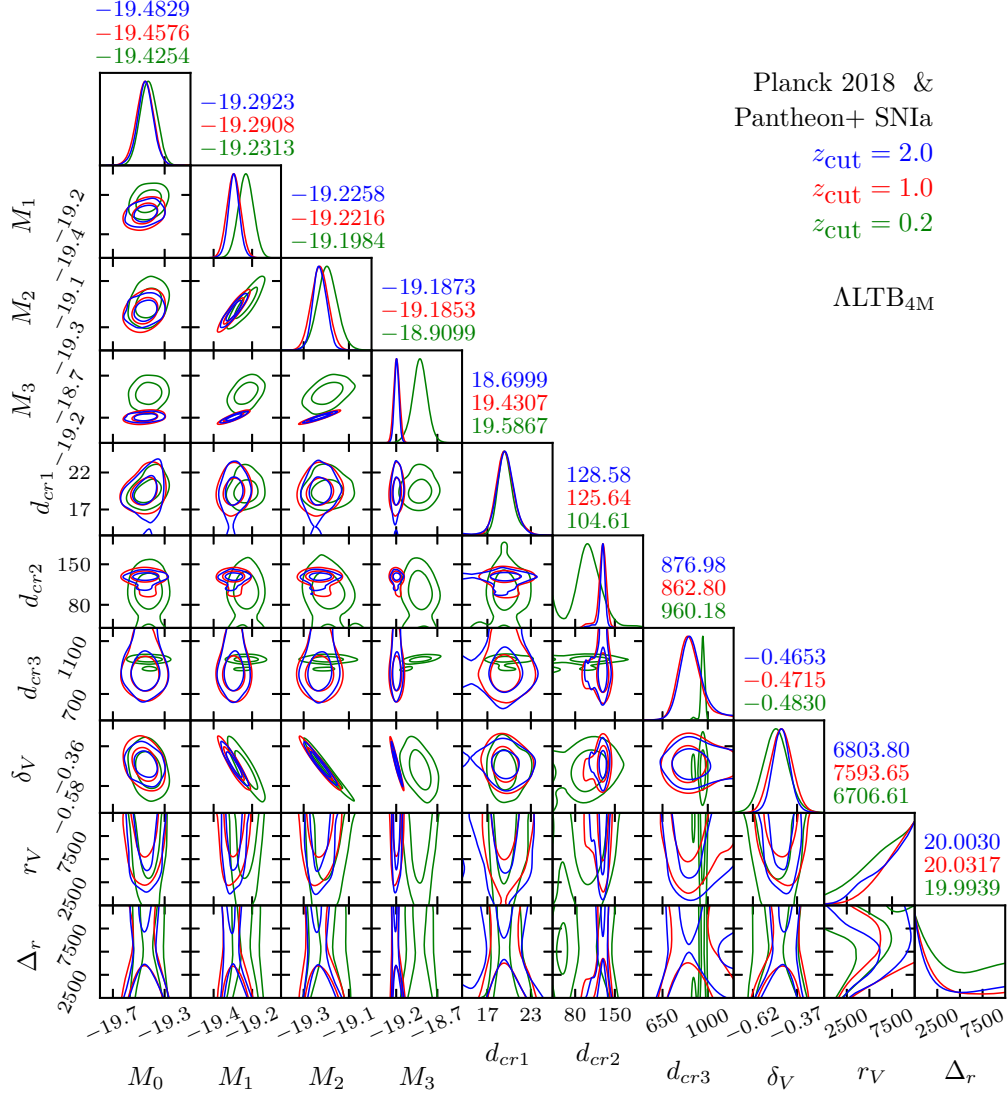


FIG. 7: The same as in Fig. 1, but for the ALTB<sub>4M</sub> model and the data of SNIa+CMB. See Sec. IV for details.

distance  $d_L(z)$ . The comoving sound horizon  $r_s(z)$  is given by [74]

$$r_s(z) = \frac{c}{H_0} \int_0^{1/(1+z)} \frac{da}{a^2 E(a) \sqrt{3(1+\eta a)}}, \quad \eta = \frac{3\Omega_b h^2}{4\Omega_\gamma h^2} = 31500 (T_{\text{CMB}}/2.7 \text{ K})^{-4} \Omega_b h^2, \quad (32)$$

where  $a = (1+z)^{-1}$  is the scale factor,  $T_{\text{CMB}} = 2.7255 \text{ K}$  [75], and  $\Omega_b h^2 = 0.02237$  from the Planck 2018 result [11]. Noting that the integration in Eq. (32) is computed at very high redshift  $z \geq z_* = 1089.92$ , the radiation cannot be ignored. In this case, the dimensionless Hubble parameter is given by [74]

$$E(a) = [\Omega_r a^{-4} + \Omega_m a^{-3} + (1 - \Omega_m - \Omega_r)]^{1/2}, \quad (33)$$

$$\Omega_r = \Omega_m / (1 + z_{\text{eq}}), \quad z_{\text{eq}} = 2.5 \times 10^4 (T_{\text{CMB}}/2.7 \text{ K})^{-4} \Omega_m h^2, \quad (34)$$

where  $h$  is  $H_0$  in units of 100 km/s/Mpc. We minimize the total  $\chi^2$ , namely

$$\chi_{\text{tot}}^2 = \chi_{\text{SN}}^2 + \chi_{\text{CMB}}^2, \quad (35)$$

to constrain the model parameters by using the Pantheon+ SNIa sample and the CMB data of Planck 2018 jointly.

Model	$M_0$	$M_1$	$M_2$	$M_3$	$d_{cr1}$	$d_{cr2}$	$d_{cr3}$	$\delta_V$	$r_V$	$\Delta_r$
$z < 0.2$										
ALTB <sub>2M</sub>	$-19.42^{+0.06}_{-0.05}$	$-19.23^{+0.03}_{-0.03}$			$19.66^{+0.50}_{-1.01}$			$-0.45^{+0.05}_{-0.06}$	$> 5439.50$	$< 5466.16$
ALTB <sub>3M</sub>	$-19.42^{+0.06}_{-0.06}$	$-19.23^{+0.03}_{-0.03}$	$-18.95^{+0.08}_{-0.07}$		$20.11^{+0.09}_{-1.54}$	$958.81^{+10.10}_{-4.73}$		$-0.44^{+0.05}_{-0.06}$	$> 5697.92$	none
ALTB <sub>4M</sub>	$-19.42^{+0.06}_{-0.06}$	$-19.23^{+0.03}_{-0.03}$	$-19.19^{+0.04}_{-0.04}$	$-18.91^{+0.08}_{-0.07}$	$19.66^{+0.56}_{-1.10}$	$104.04^{+26.42}_{-12.22}$	$959.43^{+10.41}_{-5.71}$	$-0.49^{+0.06}_{-0.06}$	$> 5941.53$	none
$z < 1.0$										
ALTB <sub>2M</sub>	$-19.45^{+0.06}_{-0.06}$	$-19.29^{+0.03}_{-0.03}$			$19.40^{+0.73}_{-0.89}$			$-0.37^{+0.05}_{-0.05}$	$> 6183.68$	none
ALTB <sub>3M</sub>	$-19.43^{+0.05}_{-0.06}$	$-19.27^{+0.03}_{-0.03}$	$-19.19^{+0.03}_{-0.03}$		$19.53^{+0.64}_{-0.92}$	$129.45^{+2.99}_{-3.99}$		$-0.50^{+0.04}_{-0.05}$	$> 5599.65$	none
ALTB <sub>4M</sub>	$-19.45^{+0.06}_{-0.06}$	$-19.29^{+0.03}_{-0.03}$	$-19.23^{+0.03}_{-0.03}$	$-19.19^{+0.03}_{-0.03}$	$19.34^{+0.82}_{-0.84}$	$127.34^{+5.59}_{-2.38}$	$869.07^{+19.68}_{-73.61}$	$-0.46^{+0.05}_{-0.06}$	$> 7154.88$	$< 1303.50$
$z < 2.0$										
ALTB <sub>2M</sub>	$-19.44^{+0.05}_{-0.06}$	$-19.29^{+0.02}_{-0.02}$			$19.24^{+0.73}_{-0.96}$			$-0.37^{+0.05}_{-0.05}$	$> 5885.65$	none
ALTB <sub>3M</sub>	$-19.44^{+0.06}_{-0.06}$	$-19.27^{+0.02}_{-0.03}$	$-19.19^{+0.02}_{-0.03}$		$19.42^{+0.71}_{-0.83}$	$129.41^{+2.94}_{-3.77}$		$-0.49^{+0.04}_{-0.04}$	$> 5158.87$	none
ALTB <sub>4M</sub>	$-19.45^{+0.06}_{-0.06}$	$-19.29^{+0.03}_{-0.03}$	$-19.23^{+0.03}_{-0.03}$	$-19.19^{+0.03}_{-0.03}$	$19.24^{+0.98}_{-0.83}$	$127.64^{+4.25}_{-2.41}$	$885.56^{+12.70}_{-99.33}$	$-0.46^{+0.05}_{-0.05}$	$> 6148.70$	none

TABLE IV: The same as in Table II, but for the data of SNIa+CMB. See Sec. IV for details.



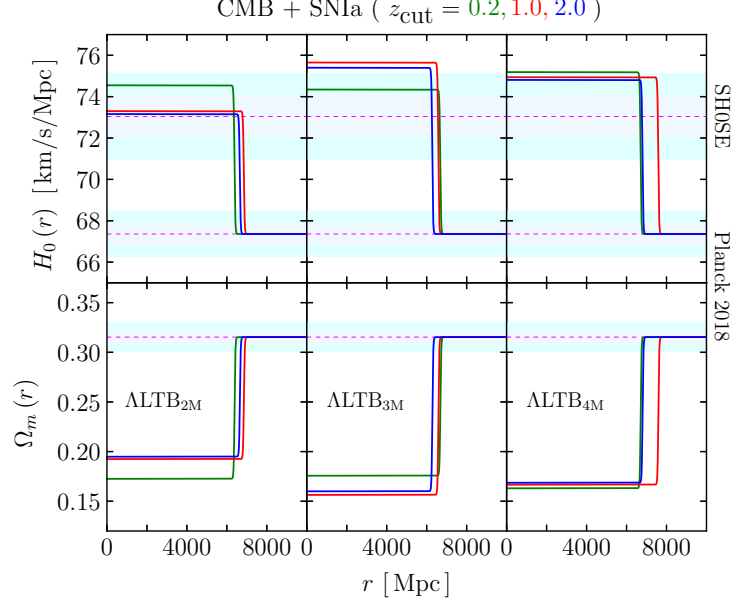


FIG. 8: The same as in Fig. 4, but for the data of SNIa+CMB. See Sec. IV for details.

Model	$\chi^2_{\text{tot, min}}$	$\chi^2_{\text{tot, min}}/\text{dof}$	$\Delta\text{BIC}_F$	$\Delta\text{AIC}_F$	$\Delta\chi^2_F$	$\ln \mathcal{B}_F$	$\Delta\text{BIC}_{P18}$	$\Delta\text{AIC}_{P18}$	$\Delta\chi^2_{P18}$	$\ln \mathcal{B}_{P18}$
$z < 0.2$										
ALTB <sub>2M</sub>	893.06	0.9460	-25.14	-39.71	-45.71	23.96	-16.48	-40.77	-50.77	15.68
ALTB <sub>3M</sub>	859.01	0.9119	-45.47	-69.75	-79.75	34.16	-36.82	-70.81	-84.81	25.87
ALTB <sub>4M</sub>	852.55	0.9070	-38.23	-72.22	-86.22	33.65	-29.58	-73.28	-91.28	25.36
$z < 1.0$										
ALTB <sub>2M</sub>	1500.37	0.8973	-20.77	-37.05	-43.05	21.50	-9.11	-36.24	-46.24	12.00
ALTB <sub>3M</sub>	1471.44	0.8811	-34.85	-61.97	-71.97	25.12	-23.18	-61.16	-75.16	15.62
ALTB <sub>4M</sub>	1460.76	0.8758	-30.68	-68.65	-82.65	27.03	-19.01	-67.84	-85.84	17.53
$z < 2.0$										
ALTB <sub>2M</sub>	1518.86	0.8956	-21.03	-37.35	-43.35	22.06	-9.83	-37.02	-47.02	12.83
ALTB <sub>3M</sub>	1490.80	0.8800	-34.20	-61.40	-71.40	25.59	-23.01	-61.08	-75.08	16.35
ALTB <sub>4M</sub>	1479.91	0.8747	-30.22	-68.30	-82.30	25.70	-19.02	-67.98	-85.98	16.47

TABLE V: The same as in Table III, but for the data of SNIa+CMB. See Sec. IV for details.

Note that the ALTB void model converges with the flat  $\Lambda\text{CDM}_{P18}$  model far outside the void. Thus, when we compute the distance priors  $\mathcal{R}$  and  $\ell_A$  for the ALTB void model,  $\Omega_m = \Omega_{m, \text{out}} = 0.3153$  and  $H_0 = H_{0, \text{out}} = 67.36$  km/s/Mpc should be used, since the CMB scale is certainly far outside the void. On the other hand, in the fiducial  $\Lambda\text{CDM}_F$  model, both  $\Omega_m$  and  $H_0$  are free model parameters.

For the model comparison, we fit the fiducial  $\Lambda\text{CDM}_F$  model to the CMB data of Planck 2018 and three  $z < z_{\text{cut}}$  SNIa subsets with  $z_{\text{cut}} = 0.2, 1.0, 2.0$ , then find  $\chi^2_{\text{tot, min, F}} = 938.769, 1543.413, 1562.208$ , respectively. For the fiducial  $\Lambda\text{CDM}_{P18}$  model,  $\chi^2_{\text{tot, min, P18}} = 943.827, 1546.602, 1565.886$ , respectively.

We fit the ALTB<sub>2M</sub>, ALTB<sub>3M</sub>, ALTB<sub>4M</sub> models to the same CMB+SNIa datasets with  $z_{\text{cut}} = 0.2, 1.0, 2.0$ , and present the  $1\sigma$  and  $2\sigma$  constraints on their free model parameters in Figs. 5 – 7, respectively. Notice that the best-fit values of their model parameters are also given in these figures. Although the

marginalized probability distributions and the  $1\sigma$ ,  $2\sigma$  contours of all the free model parameters have been plotted in Figs. 5 – 7, we also explicitly give their numerical means and  $1\sigma$  intervals in Table IV. On the other hand, we present their best-fit  $\chi^2_{\text{tot}, \text{min}}$  and  $\chi^2_{\text{tot}, \text{min}}/\text{dof}$  in Table V. Then, we calculate their  $\Delta\chi^2$ ,  $\Delta\text{AIC}$ ,  $\Delta\text{BIC}$ ,  $\ln\mathcal{B}$  relative to the fiducial  $\Lambda\text{CDM}_{\text{F}}$  and  $\Lambda\text{CDM}_{\text{P18}}$  models (labeled by the subscripts “F” and “P18” respectively), and also present them in Table V. In Fig. 8, we plot  $H_0(r)$  and  $\Omega_m(r)$  as functions of the comoving distance  $r$  by using the best-fit model parameters given in Figs. 5 – 7.

From Fig. 8, it is easy to see that the Hubble tension can be satisfyingly saved in the  $\Lambda\text{LTB}_{2\text{M}}$  void model, and can be significantly alleviated in the  $\Lambda\text{LTB}_{3\text{M}}$  and  $\Lambda\text{LTB}_{4\text{M}}$  void models within  $2\sigma$  confidence level (CL.), mainly due to the fairly deep void depth  $\delta_V \lesssim -38\%$ , even  $\lesssim -50\%$ , as shown in Figs. 5 – 7 (and supported by  $\Omega_{m, \text{in}} = \Omega_m(r=0) < 0.2$  as shown in Fig. 8).

Again, we confirm the transition of the absolute magnitude  $M$  at  $\sim 20$  Mpc found in [63] previously, and find two transitions of the absolute magnitude  $M$  at  $\sim 129$  Mpc and  $\sim 860 - 960$  Mpc, as shown in Figs. 5 – 7. The segmented  $M_i$  increases with the distance (namely  $M_3 > M_2 > M_1 > M_0$  at the critical distances  $d_{cr3} > d_{cr2} > d_{cr1}$ ), as shown in Figs. 5 – 7.

From Table IV, we can see that the constraints on the free model parameters are fairly tight (except  $r_V$  and  $\Delta_r$ ). We stress that the transitions of the absolute magnitude  $M$  are statistically significant (far beyond  $1\sigma$  uncertainties). They are not apparent changes due to large errors. On the other hand, despite the void parameters  $r_V$  and  $\Delta_r$  cannot be well constrained, they do not affect the main results since the key void parameter  $\delta_V$  can be tightly constrained in fact.

From Table V, it is easy to see that all the three  $\Lambda\text{LTB}$  models are super-strongly preferred over both fiducial  $\Lambda\text{CDM}_{\text{F}}$  and  $\Lambda\text{CDM}_{\text{P18}}$  models in all terms of  $\Delta\text{BIC}$ ,  $\Delta\text{AIC}$ ,  $\Delta\chi^2$  and  $\ln\mathcal{B}$  with “very strong” evidences, by using the data of SNIa+CMB. Clearly, these landslide preferences are overwhelming.

Let us look Table V closely. In terms of  $\Delta\text{BIC}$  ( $\Delta\text{AIC}$ ), the  $\Lambda\text{LTB}_{3\text{M}}$  ( $\Lambda\text{LTB}_{4\text{M}}$ ) model is preferred over the other two  $\Lambda\text{LTB}$  models by the data of SNIa+CMB, respectively. In terms of  $\ln\mathcal{B}$ , the  $\Lambda\text{LTB}_{3\text{M}}$  and  $\Lambda\text{LTB}_{4\text{M}}$  models are comparable. In all terms of  $\Delta\text{BIC}$ ,  $\Delta\text{AIC}$  and  $\ln\mathcal{B}$ , the  $\Lambda\text{LTB}_{3\text{M}}$  and  $\Lambda\text{LTB}_{4\text{M}}$  models are strongly preferred over the  $\Lambda\text{LTB}_{2\text{M}}$  model. In total,  $\Lambda\text{LTB}_{3\text{M}} \sim \Lambda\text{LTB}_{4\text{M}} \gg \Lambda\text{LTB}_{2\text{M}}$ . The  $\Lambda\text{LTB}$  void model with two transitions of the absolute magnitude  $M$  is the best. This hints at least one more transition of  $M$  at  $\sim 129$  Mpc in addition to the one at  $\sim 20$  Mpc found in [63] previously. Although the  $\Lambda\text{LTB}_{2\text{M}}$  model is not the best, we stress that it is still overwhelmingly preferred over both fiducial  $\Lambda\text{CDM}_{\text{F}}$  and  $\Lambda\text{CDM}_{\text{P18}}$  models by the data of SNIa+CMB.

## V. CONCLUSION AND DISCUSSIONS

Nowadays, one of the well-known serious challenges in cosmology is the Hubble tension, namely the discrepancy between the Hubble constants from the local observation of Type Ia supernova (SNIa) and the high- $z$  observation of cosmic microwave background (CMB). Here, we are interested in alleviating the Hubble tension with a local void. The key idea is to violate the cosmological principle by assuming that we live in a locally underdense void centered nearby our location. In this underdense region, one will feel a locally faster expansion rate compared to the cosmic average. In the literature, it was found that a local void cannot satisfyingly alleviate the Hubble tension, since it is not preferred over the  $\Lambda\text{CDM}$  model by the observations such as the Pantheon SNIa sample, especially in terms of the information criteria AIC and BIC. In this work, we try to alleviate the Hubble tension with a local void and transitions of the absolute magnitude  $M$ , by using the Pantheon+ SNIa sample alone or jointly with the CMB data of Planck 2018. We find that the Hubble tension can be satisfyingly alleviated, while the  $\Lambda\text{LTB}$  models are strongly preferred by the observations.

As mentioned in Secs. I and III, the key difference between the Pantheon+ SNIa sample and the other SNIa samples (e.g. DESY5, Union3, Pantheon, JLA, Union2.1, SNLS3) is the 77 Cepheid calibrated host-galaxy distance moduli provided by SH0ES, which can be used to constrain the absolute magnitude  $M$  alone (n.b. the first row of Eq. (23), regardless of  $H_0$  appeared in  $d_L$  of the theoretical model), and hence the degeneracy between  $H_0$  and  $M$  are broken, so that they can be separately constrained. Thus, it is possible to simultaneously study the Hubble tension and transitions of the absolute magnitude  $M$  by using the Pantheon+ SNIa sample. Without these Cepheid calibrated host-galaxy distance moduli provided by SH0ES, however,  $H_0$  and  $M$  are heavily degenerated in the cases of the DESY5 and Union3 SNIa samples (through a combination  $\mathcal{M} = M + 5 \log(c/H_0/\text{Mpc}) + 25$ , which can be marginalized as

a nuisance parameter). In order to study the Hubble tension, usually in the literature one has to fix  $M$  to be a constant value given by SH0ES or impose a Gaussian prior on  $M$ . But in this way, we cannot further consider transitions of the absolute magnitude  $M$ . Therefore, it is fairly difficult to use alternative SNIa samples (such as DESY5 and Union3) to independently replicate the same/similar works as in the present paper.

In this work, we have considered a phenomenological scenario combining a local void with multiple transitions of the absolute magnitude  $M$ , which significantly increases model complexity, and the risk is over-fitting the data without a compelling physical mechanism driving these transitions (we thank the referee for pointing out this issue). First, the Occam’s Razor is quantified by the Bayesian evidence, AIC and BIC. The added complexity is worthy if it can significantly improve the Bayesian evidence, AIC and BIC. As shown in Tables III and V (especially the latter), the reward of increasing model complexity is very great, while the evidences of AIC, BIC and  $\ln \mathcal{B}$  are overwhelmingly strong. Second, as shown in Tables II and IV, the transitions of the absolute magnitude  $M$  are statistically significant (far beyond  $1\sigma$  uncertainties). They are not apparent changes due to large errors and noises. Finally, there might be some physical mechanisms for transitions of the absolute magnitude  $M$ . In fact, the transition of  $M$  at  $\sim 20$  Mpc previously found in [63] is partly due to the volumetric redshift scatter bias [63, 85] (see also e.g. [50]). However, it cannot completely explain the transition of  $M$  at  $\sim 20$  Mpc, as mentioned in [63]. Thus, possible physical causes are needed for all the transitions of  $M$  at  $\sim 20$  Mpc,  $\sim 129$  Mpc and  $\sim 860 - 960$  Mpc. For instance, they might be caused by the transitions of effective gravitational “constant”  $G_{\text{eff}}$  [86–91], a broken symmetron screening mechanism [92], or a sharp feature in scalar-tensor theory potential [63]. In particular, as is well known, a varying  $G_{\text{eff}}$  is common in many modified gravity theories. It can lead to a varying/modified Chandrasekhar limit of compact stars (e.g. [64, 93]). Since SNIa explosions are closely related to the Chandrasekhar limit of white dwarfs, it is reasonable to consider possible transitions of the SNIa absolute magnitude  $M$ . Actually, there are other possible physical mechanisms to change the Chandrasekhar limit and then the SNIa absolute magnitude  $M$ , for example, a varying mass of electron, neutron or proton, a varying speed of light  $c$ , or a varying fine-structure “constant”  $\alpha$ , due to the possible coupling between the electromagnetic field and dark energy (e.g. an evolving scalar field  $\varphi$ ) [119, 120]. In the theoretical market, more physical mechanisms are waiting us to this end. Let us keep an open mind.

A local void considered here violates the cosmological principle, which assumes that the universe is homogeneous and isotropic on cosmic scales. However, the cosmological principle has not yet been well proven on cosmic scales  $\gtrsim 1$  Gpc [94]. On the other hand, the local universe is obviously inhomogeneous and anisotropic on smaller scales. In the literature, the cosmic homogeneity has been tested by using e.g. SNIa, CMB, BAO, galaxy surveys, integrated Sachs-Wolfe effect, kinetic Sunyaev Zel’dovich effect, and large-scale structure (see e.g. [37, 38, 95, 96] and references therein). However, the debate on the inhomogeneous universe has not been settled by now [18–48, 98–112]. The ALTB void firstly proposed in 1933 is still theoretically viable. On the other hand, one might be concerned with the depth of void. As noted in [48],  $\delta_V \lesssim -30\%$  is required to alleviate the Hubble tension. Actually, we find  $\delta_V \lesssim -38\%$  even  $\lesssim -50\%$  in this work. So,  $\Omega_{m,\text{in}} = (1 + \delta_V) \Omega_{m,\text{out}} \sim (1 - 38\%) \times 0.3153 \sim 0.2$ . In fact, a loose constraint on  $\Omega_m$  from galaxy cluster survey is given by  $\Omega_m = 0.20 \pm 0.04 \pm 0.09$  with  $1\sigma$  internal and systematic errors [97]. Thus, a deep local void is still consistent with large-scale structure observations.

In this work, we consider three subsets of the Pantheon+ SNIa sample with  $z < z_{\text{cut}} = 0.2, 1.0, 2.0$  following [48]. We also consider step-like transitions  $M_i$  at critical distances  $d_{cr,j}$ , and the number of  $M_i$  is chosen to be  $i = 0, 1, 2, 3$ , while the number of critical distances  $d_{cr,j}$  is correspondingly chosen to be  $j = 1, 2, 3$ . The values of  $M_i$  and  $d_{cr,j}$  are determined by fitting to the data. It is interesting to let  $z_{\text{cut}}$  float freely, and the numbers of  $M_i$  and  $d_{cr,j}$  are sampled over in the MCMC analysis (we thank the referee for pointing out this issue). But this is fairly difficult. Notice that  $z_{\text{cut}}$  is not a model parameter. It is just used to determine which SNIa will be taken into account, while  $z_{\text{cut}}$  does not directly appear in the likelihood or  $\chi^2$ . If  $z_{\text{cut}}$  floats freely, the number of SNIa at  $z < z_{\text{cut}}$  used to constrain the model parameters also floats accordingly. On the other hand, if the numbers of  $M_i$  and  $d_{cr,j}$  are also not predefined, some new techniques are needed, since the number of model parameters is not known in this case. A possible way out is to consider a series of crowded  $M_i, d_{cr,j}$  (e.g.  $j = i + 1 = 1, 2, \dots, 10$ ), and  $z_{\text{cut}}$  (e.g.  $0.1, 0.2, 0.3, \dots, 2.0$ ). Of course, it is better to instead use some new techniques to this end. But they are beyond our scope, and in order to save the length of the present paper, we leave them to the future works.

## ACKNOWLEDGEMENTS

We thank the anonymous referee for quite useful comments and suggestions, which helped us to improve this work. We are grateful to Profs. Puxun Wu, Shao-Jiang Wang, and Drs. Wang-Wei Yu, Yang Liu, as well as Han-Yue Guo, Lin-Yu Li, Shu-Yan Long, Hui-Qiang Liu, Yu-Xuan Li, Shuo-Yu Zhang for kind help and useful discussions. This work was supported in part by NSFC under Grants No. 12375042 and No. 11975046.

- 
- [1] E. Di Valentino *et al.*, Phys. Dark Univ. **49**, 101965 (2025) [arXiv:2504.01669].
  - [2] E. Abdalla *et al.*, JHEAp **34**, 49 (2022) [arXiv:2203.06142].
  - [3] L. Perivolaropoulos and F. Skara, New Astron. Rev. **95**, 101659 (2022) [arXiv:2105.05208].
  - [4] L. Verde, N. Schöneberg and H. Gil-Marín, Ann. Rev. Astron. Astrophys. **62**, 287 (2024) [arXiv:2311.13305].
  - [5] E. Di Valentino, Universe **8**, no.8, 399 (2022).
  - [6] G. Efstathiou, Phil. Trans. Roy. Soc. Lond. A **383**, no.2290, 20240022 (2025) [arXiv:2406.12106].
  - [7] E. Di Valentino *et al.*, Class. Quant. Grav. **38**, no.15, 153001 (2021) [arXiv:2103.01183].
  - [8] R. G. Cai, L. Li and S. J. Wang, Acta Phys. Sin. **72**, no.23, 239801 (2023).
  - [9] J. P. Hu and F. Y. Wang, Universe **9**, no.2, 94 (2023) [arXiv:2302.05709].
  - [10] C. L. Chang *et al.*, arXiv:2203.07638 [astro-ph.CO].
  - [11] N. Aghanim *et al.*, Astron. Astrophys. **641**, A6 (2020) [arXiv:1807.06209].
  - [12] A. G. Riess *et al.*, Astrophys. J. Lett. **934**, no.1, L7 (2022) [arXiv:2112.04510].
  - [13] A. G. Riess *et al.*, Astrophys. J. **977**, no.1, 120 (2024) [arXiv:2408.11770].
  - [14] G. Lemaître, Annales de la Société Scientifique de Bruxelles A **53**, 51 (1933);  
see Gen. Rel. Grav. **29**, 641 (1997) for English translation.
  - [15] R. C. Tolman, Proc. Nat. Acad. Sci. **20**, 169 (1934);  
see Gen. Rel. Grav. **29**, 935 (1997) for English translation.
  - [16] H. Bondi, Mon. Not. Roy. Astron. Soc. **107**, 410 (1947).
  - [17] I. Zehavi, A. G. Riess, R. P. Kirshner and A. Dekel, Astrophys. J. **503**, 483 (1998) [astro-ph/9802252].
  - [18] M. N. Celerier, Astron. Astrophys. **353**, 63 (2000) [astro-ph/9907206].
  - [19] M. N. Celerier, New Advances in Physics **1**, 29 (2007) [astro-ph/0702416].
  - [20] R. K. Barrett and C. A. Clarkson, Class. Quant. Grav. **17**, 5047 (2000) [astro-ph/9911235].
  - [21] K. Tomita, Mon. Not. Roy. Astron. Soc. **326**, 287 (2001) [astro-ph/0011484].
  - [22] K. Tomita, Prog. Theor. Phys. **106**, 929 (2001) [astro-ph/0104141].
  - [23] H. Iguchi, T. Nakamura and K. Nakao, Prog. Theor. Phys. **108**, 809 (2002) [astro-ph/0112419].
  - [24] T. J. Zhang, H. Wang and C. Ma, Phys. Rev. D **91**, 063506 (2015) [arXiv:1210.1775].
  - [25] H. Wang and T. J. Zhang, Astrophys. J. **748**, 111 (2012) [arXiv:1111.2400].
  - [26] K. Enqvist and T. Mattsson, JCAP **0702**, 019 (2007) [astro-ph/0609120].
  - [27] K. Enqvist, Gen. Rel. Grav. **40**, 451 (2008) [arXiv:0709.2044].
  - [28] J. Garcia-Bellido and T. Haugboelle, JCAP **0804**, 003 (2008) [arXiv:0802.1523].
  - [29] J. Garcia-Bellido and T. Haugboelle, JCAP **0809**, 016 (2008) [arXiv:0807.1326].
  - [30] M. N. Celerier, Astron. Astrophys. **543**, A71 (2012) [arXiv:1108.1373].
  - [31] M. N. Celerier, J. Phys. Conf. Ser. **484**, 012005 (2014) [arXiv:1203.2814].
  - [32] H. Alnes, M. Amarzguioui and O. Gron, Phys. Rev. D **73**, 083519 (2006) [astro-ph/0512006].
  - [33] M. N. Celerier *et al.*, Astron. Astrophys. **518**, A21 (2010) [arXiv:0906.0905].
  - [34] R. A. Vanderveld *et al.*, Phys. Rev. D **74**, 023506 (2006) [astro-ph/0602476].
  - [35] J. P. Zibin, Phys. Rev. D **78**, 043504 (2008) [arXiv:0804.1787].
  - [36] J. P. Zibin and A. Moss, Class. Quant. Grav. **28**, 164005 (2011) [arXiv:1105.0909].
  - [37] X. P. Yan, D. Z. Liu and H. Wei, Phys. Lett. B **742**, 149 (2015) [arXiv:1411.6218].
  - [38] Z. X. Yu, S. L. Li and H. Wei, Nucl. Phys. B **960**, 115179 (2020) [arXiv:1907.12517].
  - [39] H. Alnes and M. Amarzguioui, Phys. Rev. D **74**, 103520 (2006) [astro-ph/0607334].
  - [40] P. Sundell, E. Mörtzell and I. Vilja, JCAP **1508**, 037 (2015) [arXiv:1503.08045].
  - [41] E. G. Chirinos Isidro *et al.*, JCAP **1605**, 003 (2016) [arXiv:1602.08583].
  - [42] R. C. Keenan, A. J. Barger and L. L. Cowie, Astrophys. J. **775**, 62 (2013) [arXiv:1304.2884].

- [43] B. L. Hoscheit and A. J. Barger, *Astrophys. J.* **854**, no.1, 46 (2018) [arXiv:1801.01890].
- [44] T. Shanks, L. Hogarth and N. Metcalfe, *Mon. Not. Roy. Astron. Soc.* **484**, L64 (2019) [arXiv:1810.02595].
- [45] W. D. Kenworthy, D. Scolnic and A. Riess, *Astrophys. J.* **875**, no.2, 145 (2019) [arXiv:1901.08681].
- [46] V. V. Luković *et al.*, *Mon. Not. Roy. Astron. Soc.* **491**, no.2, 2075 (2020) [arXiv:1907.11219].
- [47] L. Kazantzidis and L. Perivolaropoulos, *Phys. Rev. D* **102**, no.2, 023520 (2020) [arXiv:2004.02155].
- [48] R. G. Cai *et al.*, *Phys. Rev. D* **103**, no.12, 123539 (2021) [arXiv:2012.08292].
- [49] D. M. Scolnic *et al.*, *Astrophys. J.* **859**, no.2, 101 (2018) [arXiv:1710.00845].
- [50] D. Brout *et al.*, *Astrophys. J.* **938**, no.2, 110 (2022) [arXiv:2202.04077].
- [51] D. Scolnic *et al.*, *Astrophys. J.* **938**, no.2, 113 (2022) [arXiv:2112.03863].
- [52] <https://PantheonPlusSH0ES.github.io>  
<https://github.com/PantheonPlusSH0ES/DataRelease>
- [53] F. Sorrenti, R. Durrer and M. Kunz, *JCAP* **2311**, 054 (2023) [arXiv:2212.10328].
- [54] F. Sorrenti, R. Durrer and M. Kunz, *JCAP* **2504**, 013 (2025) [arXiv:2403.17741].
- [55] F. Sorrenti, R. Durrer and M. Kunz, *JCAP* **2412**, 003 (2024) [arXiv:2407.07002].
- [56] M. Lopes, A. Bernui, C. Franco and F. Avila, *Astrophys. J.* **967**, no.1, 47 (2024) [arXiv:2405.11077].
- [57] R. Watkins *et al.*, *Mon. Not. Roy. Astron. Soc.* **524**, no.2, 1885 (2023) [arXiv:2302.02028].
- [58] Y. H. Sanejouand, *New Astron.* **116**, 102331 (2025) [arXiv:2312.05896].
- [59] R. G. Cai *et al.*, *Phys. Rev. D* **103**, no.12, 121302 (2021) [arXiv:2102.02020].
- [60] M. Betoule *et al.*, *Astron. Astrophys.* **568**, A22 (2014) [arXiv:1401.4064].
- [61] Y. Wang and M. Dai, *Phys. Rev. D* **94**, no.8, 083521 (2016) [arXiv:1509.02198].
- [62] A. Conley *et al.*, *Astrophys. J. Suppl.* **192**, 1 (2011) [arXiv:1104.1443].
- [63] L. Perivolaropoulos and F. Skara, *Mon. Not. Roy. Astron. Soc.* **520**, no.4, 5110 (2023) [arXiv:2301.01024].
- [64] Y. Liu, H. W. Yu and P. X. Wu, *Phys. Rev. D* **110**, no.2, L021304 (2024) [arXiv:2406.02956].
- [65] A. R. Liddle, *Mon. Not. Roy. Astron. Soc.* **377**, L74 (2007) [astro-ph/0701113].
- [66] A. R. Liddle, *Ann. Rev. Nucl. Part. Sci.* **59**, 95 (2009) [arXiv:0903.4210].
- [67] H. Akaike, *IEEE Trans. Automatic Control* **19**, 716 (1974).
- [68] G. Schwarz, *Ann. Stat.* **6**, 461 (1978).
- [69] L. Perivolaropoulos and F. Skara, *Universe* **8**, no.10, 502 (2022) [arXiv:2208.11169].
- [70] J. Torrado and A. Lewis, *JCAP* **2105**, 057 (2021) [arXiv:2005.05290].
- [71] <https://cobaya.readthedocs.org>
- [72] A. Lewis, arXiv:1910.13970 [astro-ph.IM].
- [73] <https://getdist.readthedocs.io>
- [74] L. Chen, Q. G. Huang and K. Wang, *JCAP* **1902**, 028 (2019) [arXiv:1808.05724].
- [75] D. J. Fixsen, *Astrophys. J.* **707**, 916 (2009) [arXiv:0911.1955].
- [76] R. E. Kass and A. E. Raftery, *J. Am. Statist. Assoc.* **90**, no.430, 773 (1995).
- [77] M. Kilbinger *et al.*, *Mon. Not. Roy. Astron. Soc.* **405**, 2381 (2010) [arXiv:0912.1614].
- [78] M. D. Weinberg, arXiv:0911.1777 [astro-ph.IM].
- [79] R. Trotta, *Contemp. Phys.* **49**, 71 (2008) [arXiv:0803.4089].
- [80] P. Mukherjee *et al.*, *Eur. Phys. J. Plus* **134**, no.4, 147 (2019) [arXiv:1710.02417].
- [81] A. Heavens *et al.*, *Phys. Rev. Lett.* **119**, no.10, 101301 (2017) [arXiv:1704.03467].
- [82] A. Heavens *et al.*, arXiv:1704.03472 [stat.CO].
- [83] <https://github.com/yabebalFantaye/MCEvidence>
- [84] [https://github.com/BorisNgHL/MCEvi\\_mod](https://github.com/BorisNgHL/MCEvi_mod)
- [85] W. D. Kenworthy *et al.*, *Astrophys. J.* **935**, no.2, 83 (2022) [arXiv:2204.10866].
- [86] V. Marra and L. Perivolaropoulos, *Phys. Rev. D* **104**, no.2, L021303 (2021) [arXiv:2102.06012].
- [87] G. Alestas, I. Antoniou and L. Perivolaropoulos, *Universe* **7**, no.10, 366 (2021) [arXiv:2104.14481].
- [88] D. Sapone, S. Nesseris and C. A. P. Bengaly, *Phys. Dark Univ.* **32**, 100814 (2021) [arXiv:2006.05461].
- [89] R. R. Caldwell *et al.*, *Phys. Rev. D* **73**, 023513 (2006) [astro-ph/0507622].
- [90] N. Khosravi *et al.*, *Phys. Rev. D* **99**, no.10, 103526 (2019) [arXiv:1710.09366].
- [91] G. Alestas *et al.*, *Phys. Rev. D* **105**, no.6, 063538 (2022) [arXiv:2110.04336].
- [92] L. Perivolaropoulos and F. Skara, *Phys. Rev. D* **106**, no.4, 043528 (2022) [arXiv:2203.10374].
- [93] H. Wei and Z. X. Yu, *JCAP* **2108**, 011 (2021) [arXiv:2103.12696].
- [94] R. R. Caldwell and A. Stebbins, *Phys. Rev. Lett.* **100**, 191302 (2008) [arXiv:0711.3459].
- [95] H. K. Deng and H. Wei, *Phys. Rev. D* **97**, no.12, 123515 (2018) [arXiv:1804.03087].
- [96] H. K. Deng and H. Wei, *Eur. Phys. J. C* **78**, no.9, 755 (2018) [arXiv:1806.02773].

- [97] R. Carlberg *et al.*, *Astrophys. J.* **462**, 32 (1996) [astro-ph/9509034].
- [98] M. Haslbauer, I. Banik and P. Kroupa, *Mon. Not. Roy. Astron. Soc.* **499**, 2845 (2020) [arXiv:2009.11292].
- [99] S. Mazurenko *et al.*, *Mon. Not. Roy. Astron. Soc.* **527**, 4388 (2024) [arXiv:2311.17988].
- [100] S. Mazurenko, I. Banik and P. Kroupa, *Mon. Not. Roy. Astron. Soc.* **536**, 3232 (2025) [arXiv:2412.12245].
- [101] I. Banik and V. Kalaitzidis, *Mon. Not. Roy. Astron. Soc.* **540**, no.1, 545 (2025) [arXiv:2501.17934].
- [102] B. S. Haridasu, P. Salucci and G. Sharma, *Mon. Not. Roy. Astron. Soc.* **532**, 2234 (2024) [arXiv:2403.06859].
- [103] P. K. Aluri *et al.*, *Class. Quant. Grav.* **40**, no.9, 094001 (2023) [arXiv:2207.05765].
- [104] C. Krishnan *et al.*, *Phys. Rev. D* **105**, no.6, 063514 (2022) [arXiv:2106.02532].
- [105] R. Mc Conville and E. Ó. Colgáin, *Phys. Rev. D* **108**, no.12, 123533 (2023) [arXiv:2304.02718].
- [106] P. Boubel *et al.*, *JCAP* **2503**, 066 (2025) [arXiv:2412.14607].
- [107] J. W. Moffat, arXiv:1608.00534 [astro-ph.CO].
- [108] J. W. Moffat and D. C. Tatarski, *Phys. Rev. D* **45**, 3512 (1992).
- [109] J. W. Moffat and D. C. Tatarski, *Astrophys. J.* **453**, 17 (1995) [astro-ph/9407036].
- [110] J. Moffat, arXiv:2502.20494 [astro-ph.CO].
- [111] S. Castello, M. Högbas and E. Mörtzell, *JCAP* **2207**, 003 (2022) [arXiv:2110.04226].
- [112] D. Camarena *et al.*, *Class. Quant. Grav.* **39**, no.18, 184001 (2022) [arXiv:2205.05422].
- [113] G. Montani *et al.*, *Phys. Dark Univ.* **48**, 101848 (2025) [arXiv:2404.15977].
- [114] G. Montani, N. Carlevaro and M. G. Dainotti, *Phys. Dark Univ.* **48**, 101847 (2025) [arXiv:2411.07060].
- [115] M. G. Dainotti *et al.*, *Astrophys. J.* **912**, no.2, 150 (2021) [arXiv:2103.02117].
- [116] T. Schiavone *et al.*, *Mon. Not. Roy. Astron. Soc.* **522**, no.1, L72 (2023) [arXiv:2211.16737].
- [117] C. Silva, arXiv:2312.05267 [gr-qc].
- [118] S. Vagnozzi, *Universe* **9**, no.9, 393 (2023) [arXiv:2308.16628].
- [119] H. Wei, *Phys. Lett. B* **682**, 98 (2009) [arXiv:0907.2749].
- [120] H. Wei and D. Z. Xue, *Commun. Theor. Phys.* **68**, no.5, 632 (2017) [arXiv:1706.04063].